Downloaded from gsabulletin.gsapubs.org on June 7, 2011

Geological Society of America Bulletin

Eolian dynamics and sediment mixing in the Gran Desierto, Mexico, determined from thermal infrared spectroscopy and remote-sensing data

Stephen Scheidt, Nicholas Lancaster and Michael Ramsey

Geological Society of America Bulletin 2011;123;1628-1644
doi: 10.1130/B30338.1

Email alerting services click www.gsapubs.org/cgi/alerts to receive free e-mail alerts when new articles cite this article

Subscribe click www.gsapubs.org/subscriptions/ to subscribe to Geological Society of America Bulletin

Permission request click http://www.geosociety.org/pubs/copyrt.htm#gsa to contact GSA

Copyright not claimed on content prepared wholly by U.S. government employees within scope of their employment. Individual scientists are hereby granted permission, without fees or further requests to GSA, to use a single figure, a single table, and/or a brief paragraph of text in subsequent works and to make unlimited copies of items in GSA's journals for noncommercial use in classrooms to further education and science. This file may not be posted to any Web site, but authors may post the abstracts only of their articles on their own or their organization's Web site providing the posting includes a reference to the article's full citation. GSA provides this and other forums for the presentation of diverse opinions and positions by scientists worldwide, regardless of their race, citizenship, gender, religion, or political viewpoint. Opinions presented in this publication do not reflect official positions of the Society.

Notes

© 2011 Geological Society of America

THE GEOLOGICAL SOCIETY OF AMERICA

Downloaded from gsabulletin.gsapubs.org on June 7, 2011

Eolian dynamics and sediment mixing in the Gran Desierto, Mexico, determined from thermal infrared spectroscopy and remote-sensing data

Stephen Scheidt[1,2,†], Nicholas Lancaster[2], and Michael Ramsey[1]
[1]*Department of Geology and Planetary Science, University of Pittsburgh, SRCC 200, 4107 O'Hara Street, Pittsburgh, Pennsylvania 15260, USA*
[2]*Desert Research Institute, 2215 Raggio Parkway, Reno, Nevada 89512, USA*

ABSTRACT

The Gran Desierto dune field is only partially composed of quartz-rich sands from the ancestral Colorado River. Local sources have been previously underestimated as a major source of sand because previous remote-sensing studies were limited in their capability to detect silicate minerals. Compositions of sands were evaluated in this study using a combination of laboratory thermal emission spectroscopy and thermal remote-sensing data acquired from the Advanced Spaceborne Thermal Emission and Reflection Radiometer (ASTER) instrument. The spatial interpolation of sample compositions allowed visualization of the sand transport pathways from feldspar-rich local sources by revealing gradients of composition between the dune field and surrounding local sources. The laboratory data were comparable to the remote-sensing retrievals of quartz and feldspar abundance. The mineralogical maturity of the Desierto dunes could be determined by the quartz/feldspar ratio, therefore providing a context for understanding the provenance of the Gran Desierto in relation to other Mojave and Sonoran dune fields. The composition of a previously undescribed group of dunes east of the Pinacate, the Sonoyta dunes, was measured as higher in potassium feldspar relative to the rest of the dune field. The composition of Sonoyta dunes is characteristic of other Mojave dune fields, which are more isolated near local feldspar-rich sources. South of the Pinacate, quartz-rich sand from the west admixes with feldspar-rich sand from the Sonoyta dunes to the east. The northern margin of the Gran Desierto is similarly enriched in feldspar from alluvial fans, and the coastal sand is influenced by carbonate sand that does not appear to survive transport to the inland dunes.

INTRODUCTION

For dune fields in dry lands, it is important to understand the sources of sand because the stratigraphy, geomorphology, and sand composition of these accumulations record responses to changes in climate, wind regime, average soil moisture, tectonics, sea level, and available sediment sources as the dunes cycle through periods of stabilization and reactivation. Sand may be supplied to a dune field from simple or complex sand transport corridors and will accumulate wherever the wind's transport capacity is exceeded (Kocurek and Lancaster, 1999). Field research in these regions has historically been difficult due to remote locations, inaccessibility, and cost. The work described here for the Gran Desierto is unique because it combines several decades of field work with the relatively recent development of sophisticated remote-sensing techniques to describe sand composition at the surface of the dunes.

The El Desierto de Altar (or Gran Desierto) in the Sonoran Desert region of northwest Sonora, Mexico, is currently the largest active sand sea in North America and an important eolian depositional system, wherein a number of possible local- to regional-scale sand transport pathways exist for sources of sand of varied composition (Fig. 1). Several studies have explained the history of dune emplacement by examining dune morphology (Lancaster et al., 1987; Lancaster, 1989, 1992, 1993a, 1995; Ewing et al., 2007), regional patterns of dune forms and ages (Beveridge et al., 2006), and geochemical and grain-size analysis of sand sources at sand sea margins (Kasper-Zubillaga, 2009; Kasper-Zubillaga and Carranza-Edwards, 2005; Kasper-Zubillaga and Faustinos-Morales, 2007; Kasper-Zubillaga et al., 2007, 2008). These studies have resulted in various hypotheses for the depositional history of the Gran Desierto, which include reworking of previously deposited Colorado River sediment.

Mineralogical maturity is a tool for the interpretation of sediment provenance, transport history, and weathering history of dune field sediments (Muhs, 2004). The process of dune sand maturity is a function of its source composition and the degree of physical and chemical weathering. For eolian deposits in the Mojave and Sonoran Deserts, mineralogical maturity can be defined as a compositional state that is mainly described by the relative quartz/feldspar ratio (Muhs, 2004). Several researchers have studied the dune sands of the surrounding Mojave and Sonoran Desert dune fields (e.g., Smith, 1982; Tchakerian, 1991; Sharp, 1966; Lancaster, 1993b, 1994; Zimbelman et al., 1995; Winspear and Pye, 1995; Clarke and Rendell, 1998; Kocurek and Lancaster, 1999; Tchakerian and Lancaster, 2002; Muhs et al., 2003; Derickson et al., 2008; and others), but the mineral composition and mineralogical maturity of Gran Desierto dune field as a whole have not been studied or adequately addressed. In the Sonoran and Mojave Deserts of the southwestern United States and northwestern Mexico, dune fields are commonly composed of quartzofeldspathic sands, reflecting the surrounding alluvial and fluvial source material of surrounding bedrock. A major source of sand to the Gran Desierto is undoubtedly the Colorado River. The fluvial sediments of the lower Colorado River have a quartz-rich composition (78%–85% SiO_2) originating from the quartz-rich Coconino, Navajo, and Kayenta Sandstones upstream of the Mojave and Sonoran Deserts, in northern Arizona, southeastern Utah, and western Colorado (McKee, 1979). Several dune fields along and immediately around the Colorado River originate from this sediment supply, including the Algodones dunes in southeastern California (Muhs et al., 1995; Winspear and Pye, 1995; Derickson et al., 2007) and the Parker dunes of western Arizona (Zimbelman and Williams, 2002; Pease and Tchakerian, 2003; Muhs et al., 2003). The high quartz content of the Algodones

[†]sscheidt77@gmail.com

GSA Bulletin; July/August 2011; v. 123; no. 7/8; p. 1628–1644; doi: 10.1130/B30338.1; 7 figures; 1 table.

For permission to copy, contact editing@geosociety.org
© 2011 Geological Society of America

Downloaded from gsabulletin.gsapubs.org on June 7, 2011

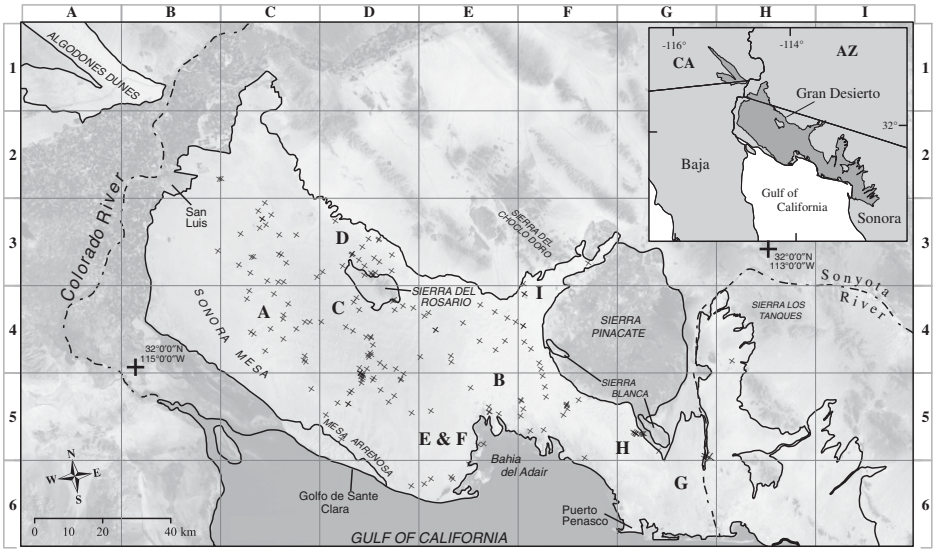

Figure 1. Location map of the Gran Desierto Mexico. The inset map shows the larger regional context of the dune field. Sample locations are marked by the "x" symbol throughout the dune field. Letters A–H on the map correspond to geographic locations of the averaged sample thermal infrared (TIR) spectra (Fig. 3), and letters A–I correspond to the composition retrievals (Table 1). Locations are referred to as: A—central dunes; B—eastern crescentic dunes; C—Rosario south; D—Rosario north; E—coastal carbonate-rich sands; F—coastal quartz-rich sands; G—Sonoyta dunes; H—southern Pinacate; I—northern Pinacate. CA—California; AZ—Arizona.

dunes (83%–88% SiO_2) and the Parker dunes (87%–90% SiO_2) led to the conclusion that these dunes are relatively mature mineralogically, where the quartz-rich source partially explains their composition (Muhs et al., 1995). In contrast, other dune fields in the Mojave Desert of California have a much higher total feldspar composition. For example, 16%–22% feldspar abundance was estimated from X-ray diffraction (XRD) peak heights for the Rice Valley dune field (Muhs et al., 2003), and an average of 51% feldspar abundance was estimated for the Kelso dunes using thermal infrared (TIR) emission spectroscopy (Ramsey et al., 1999). Both Muhs et al. (2003) and Ramsey et al. (1999) concluded that dunes in these areas are derived from local sources that have experienced minimal chemical weathering and have not been transported long distances.

This paper describes a robust quantitative analysis of thermal infrared (TIR) spectral data of the Gran Desierto to map the spatial distribution of sand composition, focusing on bulk silicate mineralogy (quartz and feldspar), which has been difficult to quantify in past studies (Blount et al., 1990). Zimbelman and Williams (2002) concluded that the determination of the quartz/feldspar ratio detected by thermal infrared remote sensing with adequate spectral and spatial resolution would have considerable use for investigations of large sand sheets and dune fields. The advantages of two different data sets are combined in mosaics of multispectral TIR data from the Advanced Spaceborne Thermal Emission and Reflection Radiometer (ASTER) satellite instrument and the high-resolution TIR emission spectroscopy of sand samples collected in the field. By mapping the spatial distribution of mineralogy, especially quartz and feldspar, we update the only previous remote-sensing study of the Gran Desierto (Blount et al., 1990) with more accurate results. We compare the Gran Desierto dune field to other geochemical studies of sands (e.g., Kasper-Zubillaga et al., 2007) and place it in the context of other regional studies of dune fields of the Mojave and Sonoran Deserts (e.g., Zimbelman and Williams, 2002; Muhs, 2004) and geomorphic studies of Desierto dunes (e.g., Lancaster, 1992, 1995; Beveridge et al., 2006).

Remote-Sensing Background

A remote-sensing–based interpretation of the Gran Desierto sand accumulation was proposed by Blount and Lancaster (1990), which drew upon field work, laboratory analysis, and reflectance spectroscopy of sand samples. For that study, Landsat 5 Thematic Mapper (TM) reflectance data were used for spectral linear unmixing analysis to delineate sand populations. The interpretations of dune mineral composition from this and other previous studies of dune areas using reflectance data (Shipman and Adams, 1987; Paisley et al., 1991; Pease et al., 1999) have been limited due to the spectral complications of visible and near-infrared (VNIR) remote sensing. It is difficult to accurately distinguish many silicate minerals because of their generally featureless spectra in the visible to shortwave-infrared wavelength region (0.45–2.35 μm), as well as the nonlinear mixing of reflected energy and particle-size effects in this wavelength region (Hapke, 1981; Mustard and Pieters, 1988). Consequently, the spatial variability of sand composition in the Gran Desierto (Blount et al., 1990; Blount and Lancaster, 1990) has remained uncertain, which is an important component of understanding the origins of the Gran Desierto dunes.

In the TIR wavelength region, mixing of emitted radiant energy is linearly related to the areal abundance of major rock-forming minerals (e.g., silicates, carbonates, and sulfates), which have diagnostic spectral absorption features (e.g., Thomson and Salisbury, 1993; Ramsey and Christensen, 1998). Linear deconvolution of TIR emission spectra has been used as an effective tool for extracting the mineralogical composition of igneous and metamorphic rocks (Feely and Christensen, 1999), meteorites (Hamilton et al., 1997), mafic and ultramafic igneous rocks (Hamilton and Christensen, 2000), granites (Ruff, 1998), volcanic rocks (Wyatt and McSween, 2002), feldspars (Milam et al., 2004), and glasses (Byrnes et al., 2007), among others. TIR remote-sensing observations have been used to identify variations in surface composition using airborne instruments on Earth (Gillespie and Kahle, 1977; Kahle, 1987; Gillespie, 1992a; Hook et al., 1994; Crowley and Hook, 1996; Hook et al., 2001; Kirkland et al., 2002), specifically for dune surfaces (Edgett et al., 1995; Ramsey et al., 1999; Bandfield et al., 2002), and TIR satellite remote sensing has been used to determine surface composition on Mars (Christensen et al., 2000, 2001, 2004; Bandfield et al., 2000; Hamilton et al., 2001, 2007; Bandfield et al., 2004; and others).

The ASTER instrument has a significant advantage in the remote sensing of Earth's geologic materials because of its moderately high spatial resolution (Instantaneous Field of View [IFOV] = 90 m), enhanced multispectral capabilities in the TIR, and global coverage (Yamaguchi et al., 1998). This study makes use of the five bands in the TIR wavelength region (8–12 μm), where silicate spectral features are common and can be analyzed from emissivity data, which were extracted from the TIR radiance of the land surface.

Downloaded from gsabulletin.gsapubs.org on June 7, 2011

TIR emissivity from ASTER has been useful in discriminating among quartzose, mafic, and granitic rocks and sediments (Rowan and Mars, 2003) and making distinctions between quartzose rock units (Rowan et al., 2005). Spectral linear deconvolution of ASTER TIR emissivity data has been used to map surface compositions at Meteor Crater, Arizona (Wright and Ramsey, 2006; Ramsey, 2002), changes in playa mineralogy at Soda Playa, California (Katra and Lancaster, 2008), and eolian sands in northern Coachella Valley, California (Katra et al., 2009). Most geologic mapping studies using ASTER data have been limited to a few scenes. However, mosaic techniques of ASTER TIR data have since been developed to expand the capability for mapping large sand seas beyond the limits of a single image footprint (Scheidt et al., 2008).

GEOLOGIC SETTING

Other studies have summarized the physiographic, tectonic, and geologic setting of the Gran Desierto dune field (Blount et al., 1990; Blount and Lancaster, 1990; Beveridge et al., 2006; Kasper-Zubillaga et al., 2007), which is important to understanding the possible sources of sediment to the dune field. The Colorado River is the largest potential source of sand for the dunes (Merriam and Bandy, 1969). The majority of the dune field is located between the Colorado River valley to the west, the Basin and Range Province to the north/northeast, and the shores of the Gulf of California to the south. The center of the dune field is situated atop thick sequences of fluvial-deltaic sediments associated with the Pleistocene Colorado River. Its western margins are separated from the Colorado River by a topographic high (100 m), the Sonora Mesa, which parallels the Colorado River and Delta. The Algodones dune field lies on the north side of the river at the northwest corner of the Gran Desierto dune field. The topographic high resulted from tectonic uplift and coalesces with the Mesa Arenosa (120 m) southeast along the coast toward the Bahia del Adair. The area west and southwest of the dune field is a widespread desert pavement surface of well-rounded pebble-sized chert, Epidote, and quartzite, indurated by silts and clays that extend underneath the sand sheets and dunes. The Gulf of California coast is characterized by intermittent playa/sabkha surfaces (along the Bahia del Adair), Pleistocene deltaic deposits, raised beaches, and outcrops of coquina (a carbonate-cemented rock composed of shell hash) (Colleta and Ortlieb, 1984). These coastal areas contribute eolian sediments composed of fine-grained quartz sand, carbonate shell hash (Ives 1959), gypsum, and salts. The alluvial fans of the Sierra del Rosario and other mountains of the Basin and Range Province along the northern edge of the dune field constitute a myriad of volcanic, sedimentary, metamorphic, and plutonic source lithologies (Ortega-Gutiérrez et al., 1992; Nourse et al., 2005), contributing alluvial sands of quartz, feldspar, biotite, and hornblende into the margins of the sand sea. East of the main dune field, the Sierra Pinacate volcanic complex (May, 1973; Wood, 1974; Gutmann and Sheridan, 1978; Greeley and Iversen, 1985; Lynch and Gutmann, 1990; Gutmann and Sheridan, 1978; and others) is dominated by basalts and is composed of numerous maar craters, lava flows, and cinder and tuff cones. The Pinacate and its alluvial drainages (arroyos) contribute sediments of varied mineralogy as well, including basalt grains, fresh phenocrysts of feldspar, and weathered rocks. Embedded and exposed among the Pinacate Quaternary and Tertiary basalts, there are older quartzofeldspathic plutons, such as the Sierra Blanca, and potassium-feldspar–rich trachytes.

The many dune groups in the Gran Desierto are hypothesized to be genetically different eolian accumulations of different age and composition, representing periods of eolian construction, stabilization, and/or reworking (Lancaster, 1992). The sand composition of the dunes in relation to these dune groups is important to understanding the history of the dune field. Grain size, grain sorting, texture, and color of the sands have been documented in previous studies (Blount and Lancaster, 1990; Blount et al., 1990; Lancaster, 1992). The major groups of dunes include a central core of star dunes, crescentic dunes that onlap the sand sheets and desert pavement to the west, linear dunes between the Sierra Pinacate and the Basin and Range, compound crescentic dunes north of the Bahia del Adair and east and south of the Sierra Pinacate, and coastal parabolic and linear dunes to the southeast.

The Sierra Pinacate volcanic complex was previously described as a topographic barrier defining the eastern limit of the dune field (Blount et al., 1990), but the Gran Desierto can actually be thought of as a continuous eolian system that extends from the Colorado River to the Sierra el Alamo far to the southeast along the coast of the Gulf of California. A group of crescentic dunes lies adjacent to the entire southern flank of the Sierra Pinacate, extending in coverage eastward to the Sierra Blanca. Between this group of dunes and the Puerto Peñasco coastline, a sand sheet with various groups of crescentic, coppice, parabolic, and linear dunes occupies the coastal plain. Much of the area is stabilized by vegetation and is, in some areas, indurated with a surface crust. Active dune forms are also intermittently present. This extension of the Gran Desierto has not been previously described and is called here the Sonoyta dunes. These eolian deposits extend to the eastern side of the Pinacate, northeast along the ephemeral Sonoyta River to the base of the Sierra Los Tanques, and as far as 120 km south along the coast to the Sierra del Alamo (Fig. 1). The crests of the linear dunes are oriented in a southwest-northeast direction, perpendicular to the coast of the Gulf of California, extending inland to the base of alluvial fans.

Approach

In order to map surface mineral compositional patterns of eolian sands in the Gran Desierto at high spatial and spectral resolution, two complementary data sets were prepared and combined: (1) a mosaic of ASTER TIR remote-sensing imagery, and (2) high-resolution laboratory TIR emission spectroscopy measurements of sand samples. In both data sets, mineral composition was determined directly from calibrated emissivity data using spectral linear deconvolution methods. Several field campaigns provided a group of regionally dispersed sand samples for a detailed, systematic spectral analysis of sand composition. At these point-locations, in situ field observations and the analysis of laboratory results served as ground-truth for the ASTER TIR remote-sensing retrievals of composition. These retrievals were extracted from a seamless, multispectral, radiometrically balanced TIR mosaic of the Gran Desierto, previously described in Scheidt et al. (2006, 2008). The laboratory spectra are very high resolution and therefore most accurately model the sand composition at these specific points. The laboratory results guided the selection of the spectral end members for the linear deconvolution of ASTER image data. These laboratory spectral end members were convolved to the lower spectral response function of ASTER and served as end members for the linear spectral deconvolution of the mosaicked image data. Because the laboratory data provided adequate spatial coverage, it was possible to spatially interpolate mineral compositions, and these were used to examine spatial trends and make comparisons directly with the spatially continuous mineral maps derived from ASTER image data. Visualization of the spatial-spectral variability of the mosaic data was possible using various transformations of the TIR imagery; here, we present a principal component analysis (PCA) for this visualization. We compare the results of laboratory and remote-sensing retrievals of composition, and the bulk mineral composition of the sands is compared to previous studies of dune

Downloaded from gsabulletin.gsapubs.org on June 7, 2011

sand composition in the Mojave and Sonoran Desert regions (Ramsey et al., 1999; Zimbelman and Williams, 2002; Muhs, 2004; Kasper-Zubillaga et al., 2007).

METHODS

Sample Preparation

Field Collection

A sand sample represents a point measurement of surface sand composition at the subpixel scale of the ASTER data. Sand samples were collected from 76 locations during field campaigns in December 2004 and March 2005, which were accurately geolocated using a real-time differential global position system (GPS). The spatial accuracy was ±2 m. Potential sample collection sites were selected based on several image products generated from Landsat and ASTER data that characterized spectral variability of the sands, such as the color variations of a decorrelation stretch of mosaicked ASTER TIR data (Scheidt et al., 2006, 2008). Sand samples were collected from the upper surface of dunes (<5 mm depth), generally the dune crest. Materials were also collected to characterize local variability of local source composition, such as sediments from playas, alluvial fans, and outcrops of volcanic and granitic rock. In addition, many sand samples have been collected by previous researchers and archived at the Desert Research Institute (DRI). Surface sand samples were selected from this archive for an additional 203 different locations, resulting in nearly complete geographic coverage of the Gran Desierto. The locational accuracy of these archived samples was determined from a comparison of field notes recorded on aerial photography to georeferenced and colocated Landsat TM satellite imagery (60 m spatial resolution) and orthophotos (www.inegi.org.mx). Accuracy for these locations is less than the ASTER 90 m spatial resolution.

Laboratory Spectroscopy and Linear Deconvolution

Thermal emission spectra of all sand samples were measured at the University of Pittsburgh's Image Visualization and Infrared Spectroscopy (IVIS) facility using a Nicolet Nexus 670 instrument at a 2 cm^{-1} wave number spectral resolution between 2000 and 400 wave number (~5–25 µm wavelength region). A detailed description of the measurement technique similar to IVIS is found in Ruff et al. (1997). Sand samples were put in copper cups and heated to 80 °C in a temperature-controlled oven for a period of 24 h. Each copper cup containing the sand sample was placed on a controlled heating stage within a sealed chamber, which was purged with nitrogen gas to minimize the spectral effects from carbon dioxide and water vapor during spectral measurement. The temperature of the cup was stabilized at 80 °C during measurement. The field of view of the instrument was ~2 cm at the sediment surface. The surface of the sand sample was scanned by the spectrometer (n = 512 scans) over a period of ~5 min per sample. These scans were subsequently averaged to reduce instrument measurement noise. Raw emitted radiance data were then processed to emissivity spectra following Ruff et al. (1997). The resulting spectra of the sand samples allow composition to be determined from a much larger number of sand grains than would be obtained from an average point count.

The bulk mineralogy of the sand samples was determined by using a linear deconvolution algorithm that models emissivity spectra as linear mixtures of pure spectral end members (Ramsey and Christensen, 1998). The best fit between the measured and modeled spectra was achieved by a chi-square minimization. The spectral end members were chosen from a library of minerals and were modeled as combinations of the spectra in proportion to their areal fractions as

$$\varepsilon(\lambda)_i = \sum_{i=1}^{n} f_i \varepsilon(\lambda)_i + r(\lambda)_i \quad \sum_{i=1}^{n} f_i = 1.0, \quad (1)$$

where ε is the emissivity of end-member i at a specific wavelength λ, f_i is the areal fraction of the end member, n is the number of end members, and r is the residual error (Ramsey and Christensen, 1998; Ramsey et al., 1999). The sum of the fractional abundances of the end members was constrained to unity. The algorithm (used iteratively) removes end members that are less than 5% in abundance or have negative abundance values (which are invalid) and remodels the mixed spectra until mineral abundances are greater than 5%.

Because of the extensive size of the dune field and the number of possible source lithologies in the area, theoretically, a large spectral library could be required to account for the compositional variations and model sample compositions. Several iterations of spectral linear deconvolution were conducted with different groups of spectral end members, beginning first with the entire combined Arizona State University (ASU) (Christensen et al., 2000) and IVIS spectral libraries. End members that were not in significant abundance in Gran Desierto sands (<5%) were eliminated in successive iterations, after which only 32 end members were ultimately identified in linear deconvolution and considered feasible. The final selection of spectral end members was indicative of typical dune sediments and the field observations of composition in the Gran Desierto dunes and surrounding source areas (Fig. 2). Spectra in the left column in Figure 2 (Figs. 2A–2F) were significant end-member fractions found in Gran Desierto samples; spectra in the right column (Figs. 2G–2N) were much less abundant and significantly limited in geographic coverage. For each of the eolian sand samples, only a few possible end members existed in significant abundance. A blackbody (emissivity = 1.0) was also included as an end member in deconvolution iterations because it accounts for differences between the spectral contrast of library end members and the sample's spectrum. Theoretically, no mineralogical information is associated with the resulting blackbody abundance; therefore, the blackbody percentage was normalized among the other detected fractional abundances (Hamilton et al., 1997). The accuracy of modeling the mineralogy of a mineral mixture using linear deconvolution in this way is known empirically but varies between studies (Ramsey and Christensen, 1998; Feely and Christensen, 1999; Wyatt and McSween, 2002). Thomson and Salisbury (1993) modeled fractional abundances of mineral mixtures with an accuracy of 5%–12%. Hamilton et al. (1997) determined plagioclase content to within 5%–10%, and Ramsey et al. (1999) determined mineralogical abundances of Kelso dune sands to within 3.1% compared to point counts of sand samples. However, inclusion of minor accessory minerals less than 5% should be avoided due to the modeling of noise in emissivity and these accuracy assessments (Ramsey and Christensen, 1998). With successful and correct linear deconvolution, the end-member fractions sum to unity, and the root mean square (RMS) error will be proportional to the noise of the spectra. Fractional end-member amounts are reported as percentages between 0% and 100% (Table 1). The average values for key areas (lettered A through I on Fig. 1 and in Table 1) were compared to retrievals of composition from ASTER (discussed later herein).

Spatial Interpolation of Linear Deconvolution Results

The laboratory results were spatially interpolated to produce mineral maps that describe the general spatial trends of bulk mineral composition of the sands in the dune field. The accuracy of the composition retrievals was considered by excluding samples with an RMS >0.009, after which the composition data were combined into a database and imported into a geographic information system (GIS). The spatial distribution of each major compositional end member was calculated (or gridded) from the irregular

Downloaded from gsabulletin.gsapubs.org on June 7, 2011

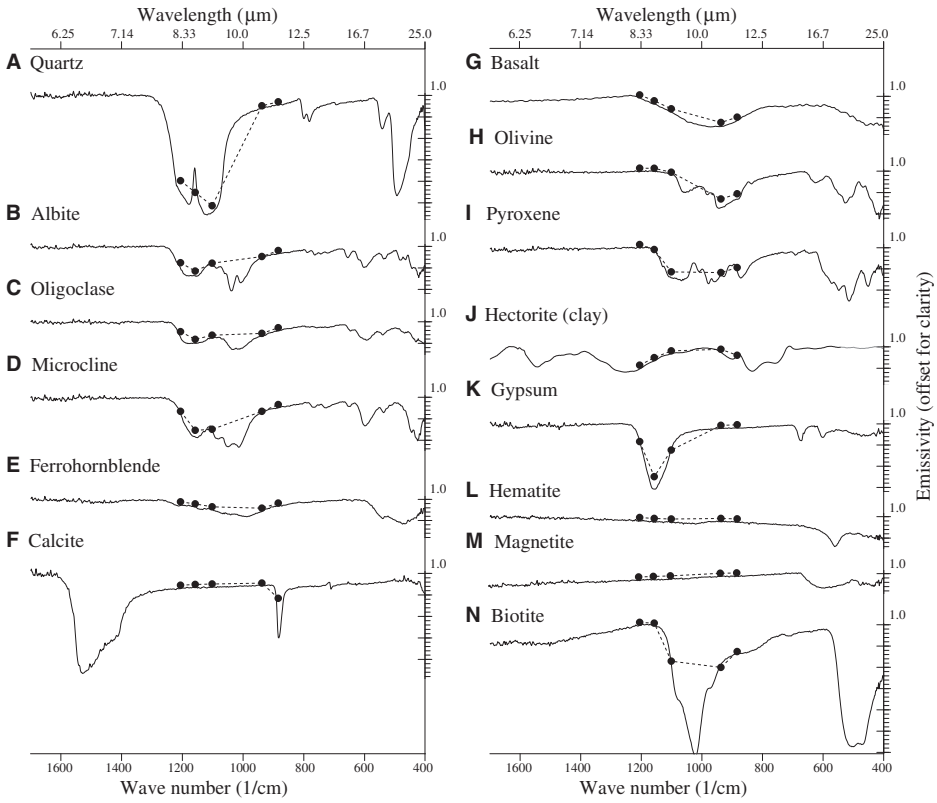

Figure 2. Emission spectra used as library end members for the linear deconvolution of laboratory spectra. Spectra in the left column were detected in significant abundance from Gran Desierto samples, where spectra in the right column were only detected in minor abundance. The dotted line with five points represents each end-member spectrum convolved to Advanced Spaceborne Thermal Emission and Reflection Radiometer (ASTER) spectral resolution. The emissivity axis is divided into major divisions of 0.1 and minor divisions of 0.02.

array of sand sampling points (shown as "x" markers in Fig. 1) using a weighted average interpolation algorithm:

$$I_j = \sum_{i=1}^{N} w_{ij} f_i, \qquad (2)$$

where I_j is the interpolated value in the grid, N is the number of points used for interpolation, f_i is the end-member fraction of the sample, and w_{ij} is the weight associated with the ith value used to compute I_j in the resulting grid of 144 × 122 nodes. Weights were determined using the inverse distance weighted technique, an exact interpolation algorithm (Davis, 1986). Because all samples were located on eolian terrain, edges of coastlines and mountain ranges were input as barriers to the spatial interpolation algorithm because these features are natural barriers to sand transport. This had the effect of increasing the weighting distance between interpolated grid nodes if points existed on either side of a topographic barrier, such as the Sierra Pinacate. The resulting contours show the spatially averaged distribution of minerals common to eolian sediment in the Gran Desierto at an average spatial resolution of 1 km × 1 km. The raw interpolations were smoothed by a 3 × 3 matrix filter to further remove the effects of small-scale compositional variability and artifacts in spatial interpolation. The spatial trends in the data were compared to the spatial distribution of composition determined from ASTER TIR imagery (discussed later herein).

TABLE 1. BULK MINERALOGY FOR THE GRAN DESIERTO AND SURROUNDING DUNE FIELDS

Sample group	*N**	Qt† (%)	Ft† (%)	Fn† (%)	Fk† (%)	Lt (%)	CO_3 (%)
Gran Desierto							
A) Central Dunes	11	78 ± 5	22 ± 4	22 ± 4	N.D.	4 ± 3	N.D.
B) Eastern crescentic	9	70 ± 4	30 ± 5	30 ± 6	BD	2 ± 2	BD
C) Rosario south	11	59 ± 8	41 ± 8	38 ± 11	3 ± 6	5 ± 4	BD
D) Rosario north	23	52 ± 8	47 ± 10	44 ± 13	3 ± 6	11 ± 9	BD
E) Coastal carbonate-rich	7	59 ± 15	41 ± 8	36 ± 9	5 ± 8	4 ± 7	31 ± 22
F) Coastal quartz-rich	10	68 ± 5	32 ± 3	32 ± 3	N.D.	2 ± 3	BD
G) Sonoyta	4	38 ± 7	62 ± 6	42 ± 12	20 ± 16	5 ± 2	N.D.
H) Southern Pinacate	5	56 ± 5	44 ± 5	34 ± 4	10 ± 7	6 ± 5	N.D.
I) Northern Pinacate	4	61 ± 11	39 ± 11	39 ± 8	N.D.	6 ± 4	N.D.
San Luis§	6	77 ± 2	23 ± 2	12 ± 2	11 ± 1	3 ± 1	BD
Puerto Peñasco§	6	55 ± 10	45 ± 4	24 ± 6	21 ± 4	4 ± 1	25 ± 12
Pinacate (northern)§	6	76 ± 1	23 ± 1	11 ± 1	12 ± 1	BD	BD
Golfo de Santa Clara§	6	83 ± 3	18 ± 2	9 ± 2	_9 ± 2	2 ± 1	21 ± 4
Kelso dunes#	13	49 ± 4	51 ± 8	31 ± 8	20 ± 4	8 ± 9	N.D.
Bristol Trough**	19	37 ± 6	73 ± 4	43 ± 6	20 ± 1	BD	BD
Clark's Pass**	16	41 ± 6	60 ± 5	39 ± 7	21 ± 2	BD	BD
Parker dunes**	6	78 ± 3	23 ± 2	12 ± 3	11 ± 1	BD	BD
Colorado River**	13	75 ± 8	25 ± 5	13 ± 6	12 ± 3	BD	4 ± 2
Algodones dunes**	1	76 ± 0	24 ± 0	14 ± 0	10 ± 0	BD	BD
Algodones dunes††	10	75 ± 1	25 ± 1	14 ± 1	11 ± 1	3 ± 1	BD

Note: Qt—total quartz; Ft—total feldspar; Fn—plagioclase feldspar; Fk—potassium feldspar; Lt—total lithics; CO_3—total carbonate minerals; BD—below detection limit; average value is <2%; N.D.—no data.

**N*—number of samples.

†Values have been normalized to the quartzofeldspathic constituents (Qt + Fn + Fk = 100%).

§Estimated from major oxides (after Kasper-Zubillaga et al., 2007).

#Measured using thermal emission spectroscopy (after Ramsey et al., 1999).

**Estimated from major oxides (after Zimbelman and Williams, 2002).

††Estimated from major oxides (after Muhs, 2004).

Downloaded from gsabulletin.gsapubs.org on June 7, 2011

Image Analysis

Selection of Image Spectral End Members

The spectral linear deconvolution results of laboratory samples were used to constrain the end-member selection for the spectral linear deconvolution of the mosaicked image data. A set of only 15 minerals produced hundreds of unique combinations of four end members or less for the Kelso dune system, where the resulting set of end members used for linear deconvolution of imagery was even fewer based on the lowest overall RMS error (Ramsey et al., 1999). Similarly for the Gran Desierto, only a few combinations of end members produced accurate, low RMS error results from the linear deconvolution of laboratory spectra. The number of spectral end members was further limited by the spectral resolution of the ASTER image data, which contain five spectral bands for the pixel-by-pixel linear spectral deconvolution. With the need to include a blackbody, the number of possible mineral end members that can be used is further reduced ($n \leq 4$). Identification of composition from ASTER was also limited by the spectral information captured by the data, which is dependent on instrument characteristics, band detection limits, the band-to-band signal-to-noise-ratio (SNR), and the spectral contrast of target minerals (e.g., Kirkland et al., 2001; and others). For example, ferrohornblende, magnetite, and hematite are all relatively difficult to detect at the subpixel level of ASTER data because they are low in abundance and have relatively few or no spectral features at ASTER wavelengths (Fig. 2).

ASTER Image Processing

The same implementation of the spectral linear deconvolution algorithm for retrieving composition from laboratory spectra was used pixel-by-pixel on the land surface emissivity extracted from the radiance mosaic using suites of both three and four end members. The results of each end-member suite were evaluated against the laboratory results. Emissivity was extracted from the corrected seamless radiance mosaic using a normalized emissivity approach (Realmuto, 1990). The assumed emissivity maximum was set to 0.96, a value typical for soils, sand, and rock. Land surface emissivity must be determined accurately from ASTER TIR remote-sensing data to retrieve the composition of dune sands. Inaccuracies in land surface emissivity obscure spectral features of surface materials or introduce spectral artifacts, which result in errors in the linear deconvolution retrievals. Consequently, much care was taken to preserve the radiometric accuracy for the mosaicked data. There are several possible approaches to normalizing and mosaicking (e.g., Martínez-Alonso et al., 2005; Hewson et al., 2005; Scheidt et al., 2008) or averaging (e.g., Hulley and Hook, 2009). The image data used for this analysis have been evaluated as accurate, derived from a seamless, high-spatial-resolution ASTER TIR radiance mosaic image (Scheidt et al., 2008). The data used incorporate an additional correction to the mosaic of TIR surface radiance (the standard AST_09T image product). Even though the AST_09T has been atmospherically corrected and is radiometrically accurate (Thome et al., 1998), these data are not corrected for reflected downwelling irradiance. This correction cannot be neglected because the Gran Desierto has a high abundance of quartz-rich dune sediments. Spectral features exhibit low emissivity values (<0.7) for ASTER bands 10, 11, and 12 (for which the effective band centers are 8.291, 8.634, and 9.075 µm wavelengths, respectively), and downwelling thermal sky radiance is reflected from the land surface back to the sensor (Kirchhoff's law) at these locations. This reflected energy reduces the spectral contrast measured by the sensor and adversely affects the spectral shape of land surface materials. This in turn adversely affects the accuracy of the retrievals of mineral composition. To reduce these effects, a correction of AST_09T similar to the iterative correction described in Gillespie et al. (1998) was developed for this study and is equivalent to the nominal correction of reflected downwelling irradiance suggested by Gustafson et al. (2006). For quartz-rich dune sediments in the core of the Gran Desierto, an average TIR radiance correction was no more than ≈0.7 Wm^{-2} μm^{-1} sr^{-1} for bands 10, 11, and 12 and improved the spectral shape of the emissivity spectra. Correction in bands 13 and 14 was negligible because reflection of downwelling irradiance is low at these wavelengths for the average surface composition in this area. Overcorrection of reflected downwelling radiance is prevented by limiting the algorithm to three iterations.

Land surface emissivity is also available as a standard product (AST_05), which is generated by the Temperature Emissivity Separation (TES) algorithm and corrects for the reflected downwelling irradiance (Gillespie et al., 1998), although the data's performance has varied through time with different versions of the TES algorithm (Gustafson et al., 2006). Early versions of the AST_05 data were found not to mosaic well for the Gran Desierto, leaving seam boundaries in the mosaic. Consequently, manual emissivity estimation using the AST_09T was preferred (Scheidt et al., 2008). Since that time, changes have been made to the TES algorithm, e.g., the threshold classifier was removed (Gustafson et al., 2006), and the AST_05 may be considered an improved product. The North American ASTER Land Surface Emissivity Database (NAALSED) is a mosaicked AST_05 emissivity product and provides coverage of the Gran Desierto (Hulley et al., 2008; Hulley and Hook, 2009). The NAALSED emissivity data have been validated over sand dune sites in the field to within 1.6% (Hulley et al., 2009). Our mosaicked ASTER TIR emissivity product, which includes clear scenes only, a reflected downwelling radiance correction, and no time-averaged emissivity values, was shown to be more accurate with respect to the retrieval of surface mineral composition using spectral linear deconvolution (described in the results section).

The clear-sky, corrected AST_09T radiance mosaic was used to generate image transformations for the visualization of the entire dune region. A decorrelation stretch (DCS) (Gillespie, 1992b) was previously generated from the radiance mosaic data for the field work completed here (Scheidt et al., 2008), and a principal component analysis (PCA) stretch (Richards, 1999) was also used to examine the spectral variability of the entire dune field. These transformation techniques were modified to include only the spectral data from arid land surface materials. Water, heavily shaded sides of mountain ranges, and dense vegetation (found in cultivated areas of the Colorado River valley) were masked from the transformation algorithms to enhance the spectral variability of exposed geologic materials (i.e., dunes, alluvial fans, and rock outcrops). The effect of sparse vegetation in the Gran Desierto region was ignored but is assumed to be low enough in areal coverage as not to greatly affect the statistics of the image transformation. The original ASTER images chosen were selected because of their low vegetation values (Scheidt et al., 2008). Low vegetation in the selected scenes was verified by the low reflectance values in the near-infrared (ASTER band 3) and low normalized differentiated vegetative index (NDVI) values. The data transformations highlight compositional information as color variations and surface temperature as intensity variations (Gillespie, 1992b; Ramsey et al., 1999). All five ASTER TIR bands were used in the PCA transformation (Richards, 1999), where the first principal component (PC) band is influenced by larger-scale spectral variance, mostly due to quartz, and temperature. PC band 5 contained the smallest-scale variations and contains the majority of noise in the data. The middle PC bands contain mostly emissivity information and composition variability. The best visualization was found to be PC bands 4, 3, and 1 placed in red, green, and blue channels, respectively, to display a false-color composite image. The

Downloaded from gsabulletin.gsapubs.org on June 7, 2011

middle PC bands 4, 3, and 2 do not produce a significantly different result. After a hue, saturation, and value (HSV) transformation (Kruse and Raines, 1984), the hue of the false-color composite was adjusted so that color values compared directly to the previous DCS and the false-color composite of the deconvolution results.

RESULTS

The results from spectral linear deconvolution of laboratory spectra of samples and TIR remote-sensing imagery reveal clear distinctions between dune sands from various regions. The primary data set used to describe accurate composition of the Gran Desierto sands was the laboratory data, whereas the spatial distributions are best revealed by satellite imagery, which supplements the spatial trends of the interpolated point-locations of sample composition.

Laboratory Spectra and Composition Retrievals

To summarize the large volume of data and reduce small-scale variability, the spectra and the compositional retrievals from individual samples are shown as averages, with respective standard deviations, by geographic area (Table 1; Fig. 3). The average compositions of different dune groups are presented alongside bulk mineralogy results from other regional geochemical studies of the Mojave and Sonoran Deserts (Table 1). Spatial trends in the average bulk mineralogy (Fig. 4) are apparent from the spatially interpolated laboratory retrievals, which were essentially generated from a moderate-spatial-resolution, but hyperspectral, TIR data cube. The most common spectral end members determined by laboratory analysis in decreasing order of average areal abundance were: quartz > plagioclase feldspar > potassium feldspar >> carbonate >> ferrohornblende. Various end-member suites were tested against the image deconvolution algorithm, and local variability in composition was observed within the sample suite. Adjacent sand populations were expected to be similar because of the ways that eolian processes physically redistribute and mix sand (i.e., deflation, winnowing, variable transport rate, and direction), and this did not always result in obvious distinctions at the scale of sampling or ASTER remote-sensing data.

Comparison of Laboratory and Image Composition Retrievals

Observing the constraints for the number of end members that were found in significant abundance from the laboratory analysis of sands,

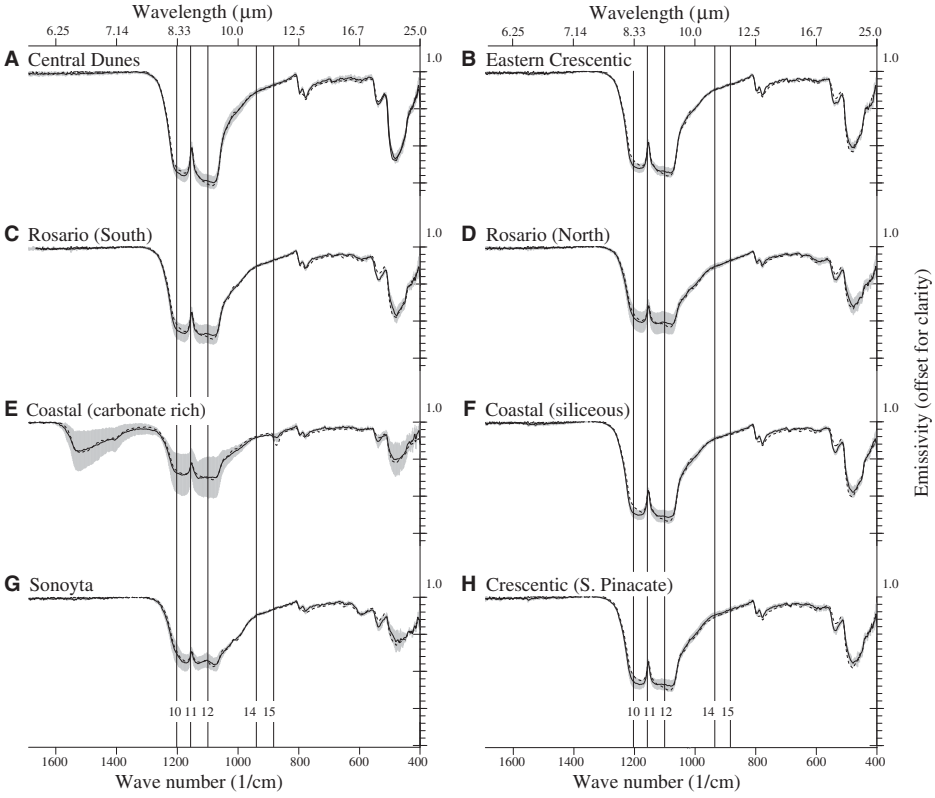

Figure 3. Laboratory thermal emission spectroscopy results from Gran Desierto samples displayed here as average spectrum (solid black line) by geographic regions corresponding to letters on the map in Figure 1. The range of upper and lower limits of averaged emissivity is shown to examine the spectral variability of the samples (gray zone). The bulk compositions of the spectra were modeled successfully using the chosen end-member suite (average root mean square [RMS] error <0.007), where the residuals are seen in the deviations from the average modeled spectrum (dotted line). Refer to Table 1 for composition retrievals. Vertical lines show the location of Advanced Spaceborne Thermal Emission and Reflection Radiometer (ASTER) band-passes. The emissivity axis is divided into major divisions of 0.1 and minor divisions of 0.02.

a three-end-member suite of quartz, plagioclase, and potassium feldspar was selected to produce the final ASTER image deconvolution results (average RMS = 0.007) to within an average accuracy of 10% (Fig. 5). The average mineral abundances were directly compared between the laboratory results and the retrievals of composition from the image analysis for the nine groups of samples (Fig. 6). ASTER retrieved quartz abundance within the accuracy expected using linear deconvolution of lower-spectral -resolution data, where this error was less than 10% for the average quartz abundance. The average underestimation of quartz abundance for all samples was 1% ($\sigma = \pm 1\%$). Total feldspar had an average overestimation of 10% ($\sigma = \pm 2\%$). The highest error occurred for coastal carbonate-rich sands, which had a 27% ($\sigma = \pm 7\%$) overestimation in total feldspar compared to laboratory retrievals. The error is due to the fact that coastal carbonate-rich sands could not be modeled correctly if a carbonate spectral end member was included in the image deconvolution iterations. A carbonate spectral end member resulted in 0% abundance in all areas and had high overall RMS error, even though shell hash and other sand-sized carbonates were easily and frequently seen in hand samples collected in the field from coastal areas. The laboratory spectra from samples in this area had significant local variation in carbonate retrieval between 9% and 53%. Unfortunately, the ASTER data do not have enough spectral resolution (5 spectral bands) to determine the carbonate content in this case. The carbonate spectral end member is relatively featureless in the ASTER spectral range of 8–12 μm, with the exception of the absorption feature at ~11.3 μm, which is quite shallow in the laboratory spectra of the samples. Consequently, carbonate abundance is more

Downloaded from gsabulletin.gsapubs.org on June 7, 2011

likely to be modeled as blackbody (ε = 1.0), which was normalized in the final results. Areas of very high carbonate abundances are probably limited to small areas along the coast. Because of the very low competency of carbonate grains with respect to the dominant quartzofeldspathic sand, carbonate is rapidly broken down with increasing distance from the coast and is not a significant component of the inland Gran Desierto dune sands. This is seen by the decrease in carbonate spectral features at ~1522 cm^{-1} and 883 cm^{-1} of the laboratory spectra for the samples and the retrieved carbonate abundance (Fig. 7). Over a distance of 2 km in the northeast direction, a transition occurs from the coastal plain of the Bahia del Adair (30% carbonate) to the dunes located inland near the Sierra Pinacate (less than 4% carbonate). In the crescentic dunes, 5 km inland from the sand sheet, carbonate was not detectable in samples.

Plagioclase feldspar was overestimated by an average of 21% (σ = ±4%) in the image deconvolution, where potassium feldspar was overestimated by an average of 3% (σ = ±4%) overall. The variability in the accuracy of individual samples is a direct result of (1) comparing data between the scales of ground sampling and remote sensing, (2) the variability in emissivity errors of TIR image pixels due to scan line and measurement noise, (3) residual atmospheric effects on retrieved emissivity, and (4) the limitations of modeling feldspar mineralogy associated with ASTER spectral resolution (five band-passes in the TIR wavelength region). In the case of the latter, an additional band between 9.075 and 10.657 µm improves the identification of feldspar minerals (e.g., Kahle, 1987; Ramsey et al., 1999; Ramsey and Rose, 2010; Scheidt et al., 2010a). Even though the abundance of plagioclase may be overestimated, the general comparison between laboratory and ASTER satellite retrievals showed an overall direct 1:1 relationship. Inaccurate results of the image analysis can probably be explained by unmodeled end members, such as carbonate in coastal regions and lithic content in sands for other areas. Accurate retrievals were observed for potassium feldspar in the Sonoyta dunes area, the central dunes, and the eastern crescentic dunes. The retrievals of mineral composition from this ASTER TIR emissivity mosaic were also compared to retrievals from the NAALSED averaged emissivity product. Most of the results compared similarly (Fig. 6E), which increases confidence in the spatial patterns of mineralogy seen from the image analysis results. Slightly higher RMS error was observed using NAALSED emissivity; plagioclase was similarly overestimated by 20%; and microcline was undetected except for some areas of the Sonoyta dune area.

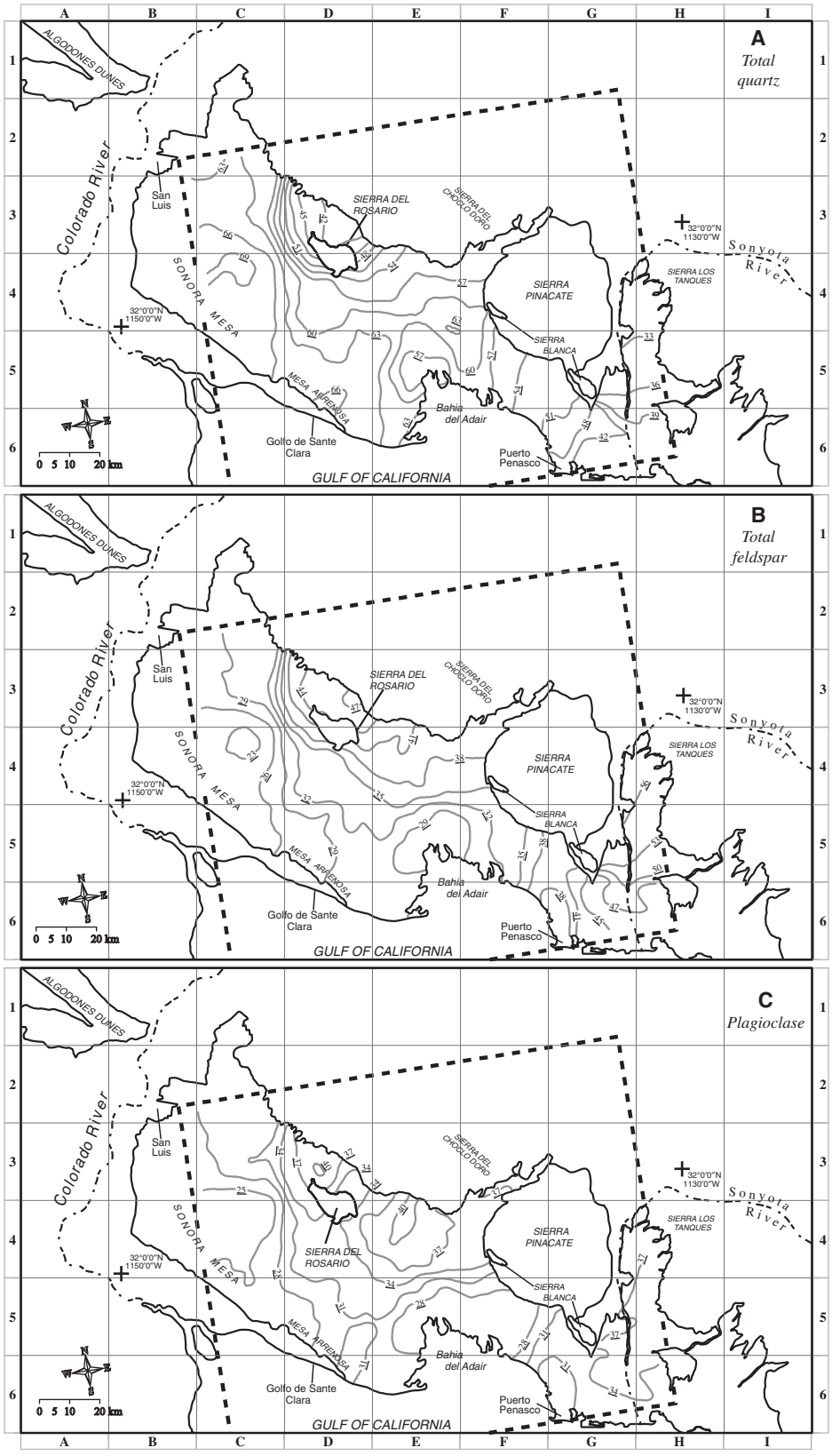

Figure 4 (*on this and following page*). Spatial interpolations of composition retrievals from laboratory thermal infrared (TIR) emission spectroscopy. The boxed outline (dashed line) shows the limits of spatial interpolation. The contour interval is 3%.

Downloaded from gsabulletin.gsapubs.org on June 7, 2011

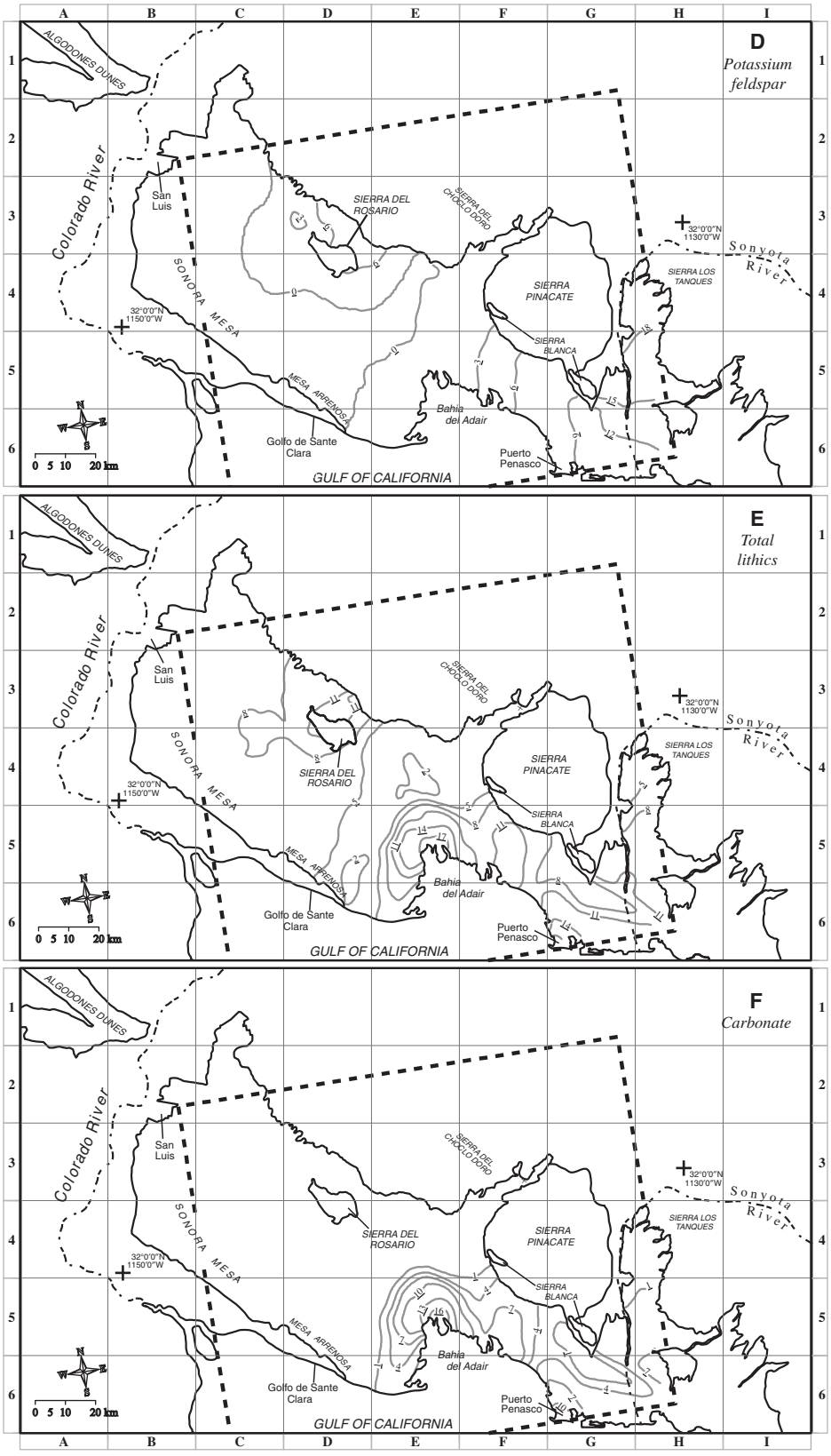

Figure 4 (*continued*).

Spatial Distribution of Composition from ASTER

The end members chosen captured the majority of the spectral variability at ASTER resolution and appear to have spatial distributions of mineral abundance retrievals that are similar to the trends exhibited from laboratory results. The fractional end-member images (Figs. 5A–5D) resulting from the image deconvolution can be directly compared to the mineral abundance maps generated from laboratory data (Figs. 4A–4D). The quartz end-member image (Fig. 5A) compares well to the contour map of the total quartz abundance, which is equivalent to the sum of quartz and chert laboratory end-member distributions (Fig. 4A). The plagioclase image (Fig. 5C) was generated using the albite end member and is comparable to the sum of sodium and calcium feldspar laboratory end-member distributions (Fig. 4C). The potassium feldspar image and laboratory interpolation were both generated using the microcline end member (Figs. 4D and 5D). The total feldspar image (Fig. 5B) is equivalent to the sum of the albite and microcline images and is comparable to the total feldspars in laboratory data (Fig. 4B). The most striking observation apparent from these data is that quartz abundance is highest in the western crescentic dunes and the adjacent star dunes (Fig. 5A, row 4, column C) as well as the eastern crescentic dune group (Fig. 5A, rows 4–5, columns E–F). Feldspar distribution is inversely proportional to quartz, with the higher values occurring in the dunes surrounding the Sierra del Rosario and in the Sonoyta dunes area. The potassium feldspar fractional image (Fig. 5D) shows higher abundance in the Sonoyta dune area east of the Sierra Pinacate and was similar to the trends in the laboratory retrievals (Fig. 4D).

An attempt was made to maximize the compositional information extracted from the image deconvolution and its accuracy by executing multiple iterations of different end-member suites. If a "mafic" end member such as olivine, augite, or basalt was used as a fourth end member, the image linear deconvolution produced competing fractional images between microcline and the mafic end-member image near the Sierra Pinacate. Quartz and albite fractional images generally remained unchanged regardless of inclusion of the fourth end member. Volcanic composition was not identified in high abundance from laboratory spectra of sand samples, although these components were visible in small quantities from hand samples. An abundance of basaltic grains is plausible in dunes near the Sierra Pinacate because grains were readily observed in the field to be actively saltating through

Downloaded from gsabulletin.gsapubs.org on June 7, 2011

topographic lows between dunes. With the inclusion of a fourth mafic end member, the agreement of potassium feldspar retrievals was underestimated with respect to laboratory retrievals for samples from the Sonoyta dunes and Sierra Pinacate areas and overestimated in quartz-rich areas like the central dunes. Potassium feldspars (microcline, orthoclase, and sanidine) are likely end members from the surrounding source rocks such as the Sierra Blanca, a group of Proterozoic metamorphic rocks (quartzites, gneiss, schist, and amphibolites) mostly obscured by the much younger Quaternary basalts (Watkins, 2003; Nourse et al., 2005). The Sonoyta River draining the Basin and Range and the Sierra Pinacate is also a likely source of both potassium feldspar as well as volcanic sands.

The better and more conservative results for dune sands were obtained using the three-mineral end-member suite of quartz, albite, and microcline (as well as a blackbody end member) because of the agreement between laboratory and ASTER retrievals of composition. Inclusion of a fourth end member in the linear deconvolution of the ASTER image data did not accurately reproduce the laboratory retrievals of composition of the dune sands. Both three- and four-end-member suites produced similarly low levels of RMS error. The three-end-member suite resulted in an RMS error image that averaged 0.007, similar to laboratory results, and was contrast-stretched to show the generally featureless distribution of error (Fig. 5E). Areas with higher RMS error are due to a lack of mafic or carbonate mineral end members used in the ASTER data deconvolution. At the spectral resolution and spatial scale of ASTER (~90 m), the four-end-member suite may characterize the region's broader surface composition, which includes noneolian sand materials, such as the pebble- to cobble-sized basalt fragments that are abundant in some of the interdune areas of the Sierra Pinacate (estimated at 20% from surveys in the field of individual pixel areas).

Principal Component Analysis of ASTER TIR

The PCA analysis captures the full spectral variability of the ASTER TIR and was found to be very useful in distinguishing overall compositional variation (Fig. 5F). The crescentic dunes in the west and the southwestern portion of the star dunes (Fig. 5, row 4, columns C–D), and the eastern crescentic dunes (Fig. 5, row 5, columns E–F) have the highest red color value in the scene. These areas correspond to the highest quartz content and compare closely to the quartz distribution of image and laboratory data (Figs. 3A and 6A). Linear and parabolic dunes

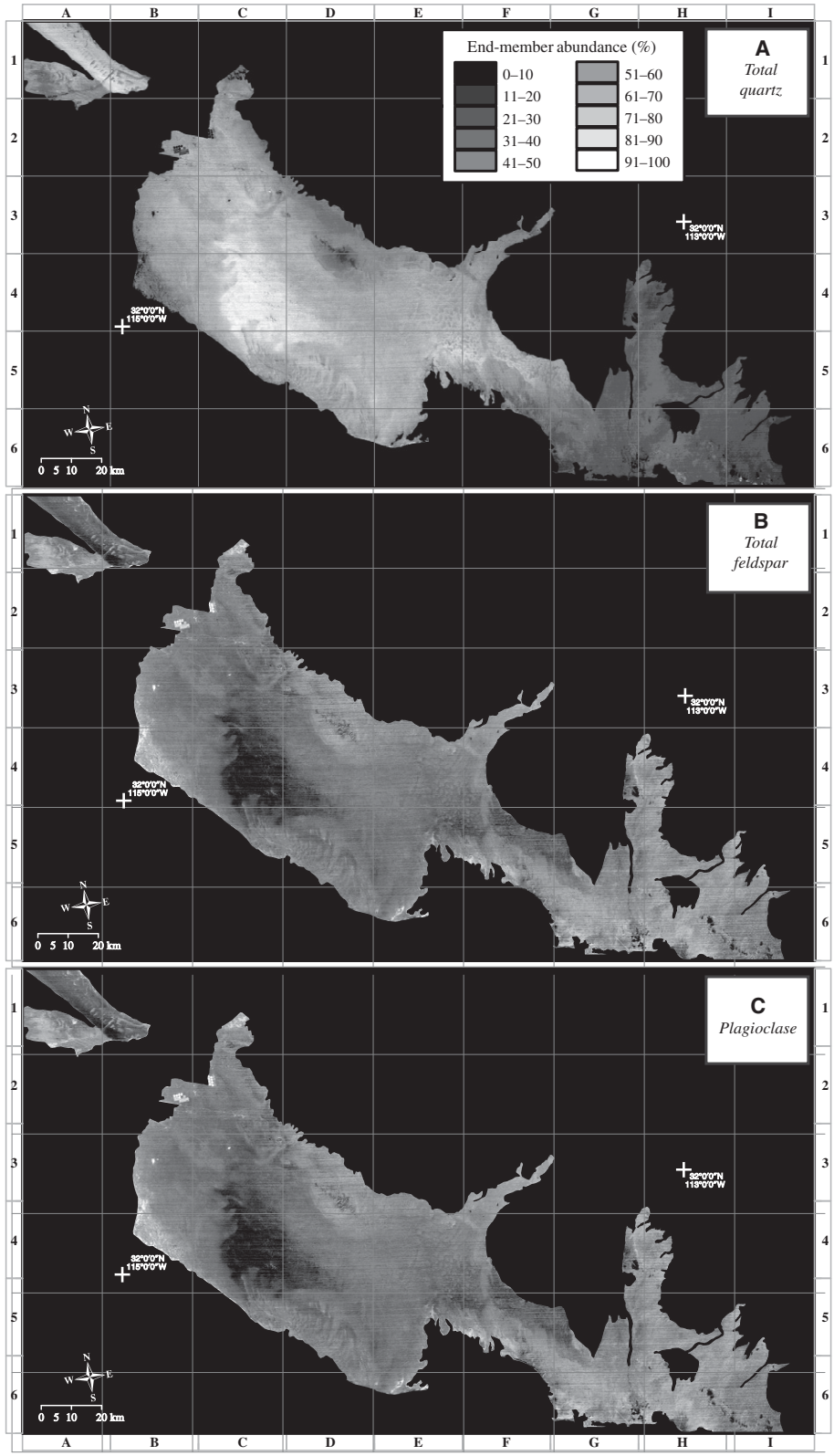

Figure 5 (*on this and following two pages*). Spectral linear deconvolution results from Advanced Spaceborne Thermal Emission and Reflection Radiometer (ASTER) image data. Results presented here used a suite of three spectral end members and generated the following fractional mineral abundance images: (A) total quartz; (B) total feldspar, which is plagioclase feldspar + potassium feldspar; (C) plagioclase feldspar.

Downloaded from gsabulletin.gsapubs.org on June 7, 2011

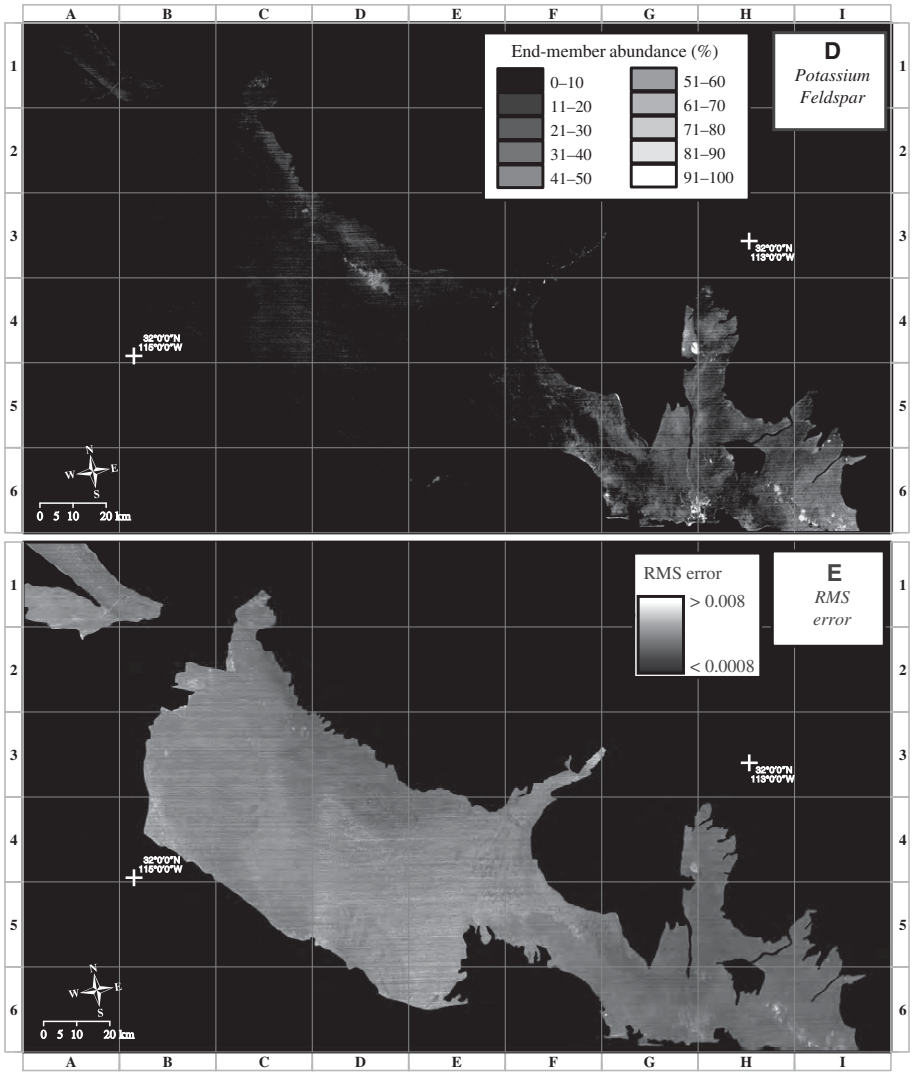

Figure 5 (*continued*). (D) potassium feldspar. (E) The resulting root mean square (RMS) error image, shown as a highly contrast stretched image between 0.0008 and 0.008, averaging 0.007.

southeast and east of the Sierra Pinacate (Fig. 5, rows 4–6, columns G–I) have distinct green and blue color in the PCA, which correspond to the admixing of locally sourced granitic and volcanic material. Alluvial fans to the north have similar feldspar-rich composition (Fig. 5, row 3, column D). The complex crescentic dunes south of the Sierra Pinacate (Fig. 5, row 5, columns F–G) have a yellow color showing the mixing of quartz- and feldspar-rich sands in a transitional zone between sand populations of the Sonoyta dunes and eastern crescentic dunes. Color variations are blue, magenta, and purple along the coast, especially around the Bahia Adair, highlighting the various evaporite compositions, carbonate-rich sands, and vegetation admixed with quartz sand. The PCA analysis captures spectral variation in ASTER band 14 that is not modeled in the linear deconvolution. Vegetation mixed at the subpixel level with quartz sand is responsible for the magenta color that appears near agricultural areas at the edge of the Colorado River valley (Fig. 5, rows 2–4, column B). Delineations of dune groups (modified after Lancaster et al., 1987; Lancaster, 1992, 1993a, 1995) are superimposed on the PCA image in order to visualize the relationship of these units with composition (discussed in the following section).

DISCUSSION

Composition of Dune Groups

The overprinting of dune patterns and spatial distributions of mineralogy make interpretation of an eolian system's emplacement history a formidable problem. A dune pattern reflects the effects of present and past climate conditions and the wind regime responsible for its emplacement. The morphological delineations of dune groups do not correlate exactly with composition modeled from ASTER remote sensing (Fig. 5F), suggesting that not all dune construction events correlate with unique sources of sand composition. A genetically unique sand population may span more than one dune generation, and a single dune morphological unit may be composed of multiple compositionally different sand types. This study infers that ancestral Colorado River sediments, sand derived from the present-day Colorado River valley, and deflationary material from the Sonora Mesa and Mesa Arenosa have been reworked in place, most likely in dune groups A and C (Fig. 5F). Western crescentic dunes (group C) have the highest likelihood of being composed of quartz-rich ancestral sediments from the Colorado River. Central star dunes (labeled as A) clearly show a gradient of increasing quartz abundance with distance from local sources of feldspar. The composition of the eastern crescentic dunes (group B5) transitions from high quartz-rich sand supplied by a coastal source to sand that is feldspar-rich derived from local sources in the north. The Sonoyta dune area (group D) is highly influenced by feldspar from local sources. Our laboratory results characterize coastal sands as a bimodal source containing both short-lived immature carbonate-rich sand and quartz-rich neritic sands that migrate in patches (group B1) inland. The Rosario dunes, such as group B4, are highly influenced by locally derived plagioclase and dark lithic abundance, where groups B5 and B3 south of the Sierra Pinacate sands are influenced by the Sonoyta dunes source, which is rich in local sources of potassium feldspar.

Quartz-Rich Dunes in the Main Dune Field

The central dunes (Fig. 1, location *A) and the eastern crescentic dunes north of the Bahia Adair (Fig. 1, *B) have the highest quartz content in the Gran Desierto (83%); this was confirmed by both spatial trends of sample interpolations and the ASTER image analysis. This area includes the westernmost star dunes and the reversing dunes at the western margin of the dune field. Quartz concentration decreases in a northeasterly direction in the central sand sea toward alluvial fans, as well as in an easterly direction across the sand sheet toward the eastern crescentic dunes (B2, B5), which average 70% quartz. The remaining fraction of sand is composed mostly of feldspar, which is higher than determined by previous studies using remote sensing and point counts (Blount et al., 1990).

Downloaded from gsabulletin.gsapubs.org on June 7, 2011

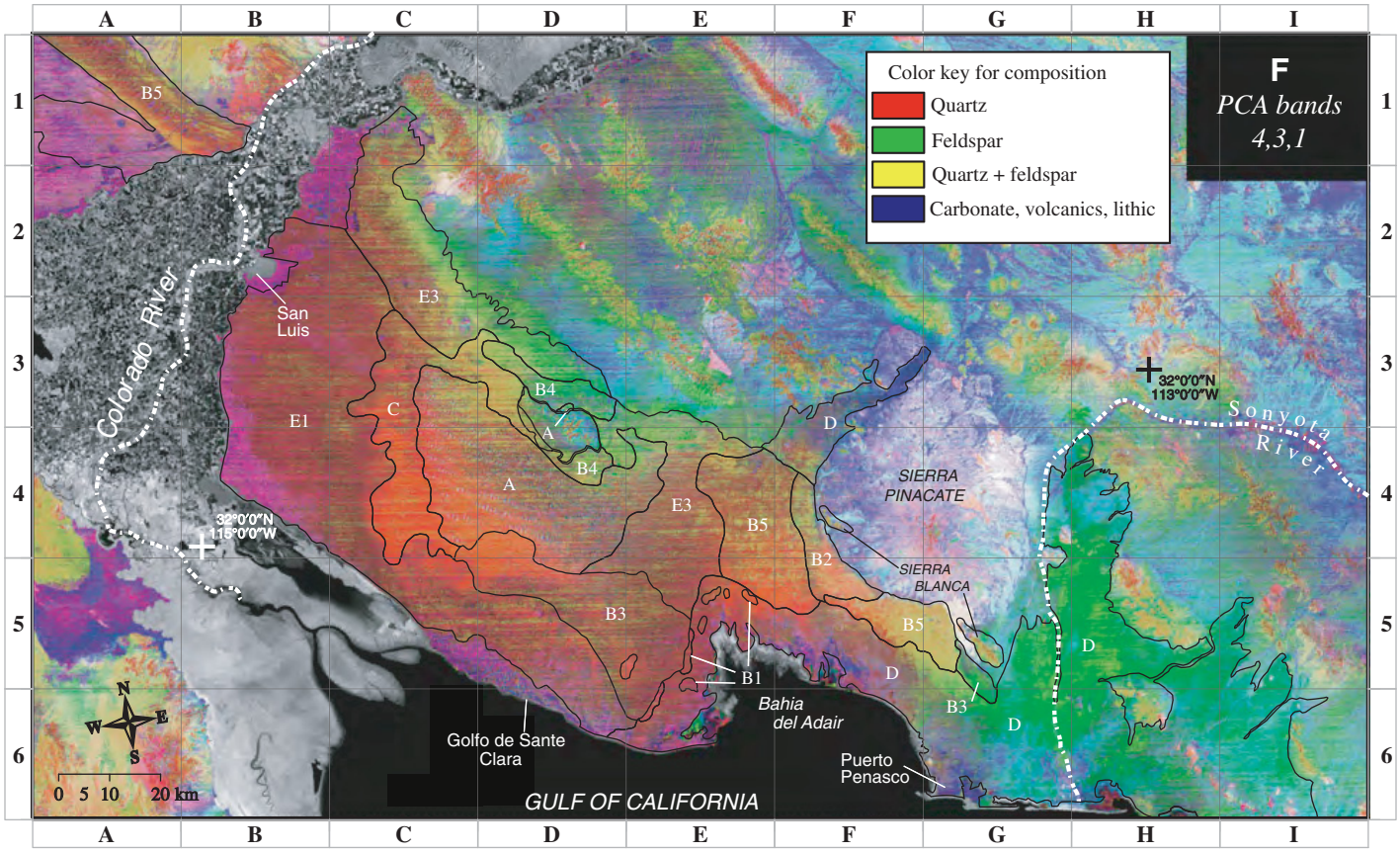

Figure 5 (*continued*). (F) Spectral variability is summarized using the principal component analysis (PCA) image described in the text (see next page). Colors correspond to compositional variations. Overlain are delineations of dune groups (modified after Lancaster, 1995). The dune types labeled by the white symbols printed within the map are: A—star dunes; B1, B2—active simple crescentic dunes; B3—large relict crescentic dunes, stabilized by vegetation; B4—coalescing multiple generations of largely relict crescentic dunes; B5—compound/complex crescentic dunes; C—reversing dunes with active crescentic dunes on margins of the area, with stabilized and relict crescentic dunes in topographically lower areas; D—linear and parabolic dunes, largely vegetated; E1—sparsely vegetated, low-relief sand sheets; E2—moderately vegetated sand sheets, 2–3 m local relief; and E3—undifferentiated sand sheets.

The concentration of total lithics for these areas is low, composed mostly of ferrohornblende in small amounts for the central dunes (~3%–7%); a variety of lithics (indistinguishable rock fragments) were detectable in very low abundance for the eastern crescentic dune area. The spectral variability among samples was lowest in these areas (Figs. 3A and 3B; Table 1, rows A and B). The Gran Desierto's central dunes area probably inherited high quartz content from ancestral Colorado River sediments in a similar way to the Parker dunes and the Algodones dunes (see Table 1). High quartz content (77%) near San Luis (Kasper-Zubillaga et al., 2007), which is in close proximity to the Colorado River, confirms this conclusion. The eastern crescentic dunes are likely supplied by input of active quartz-rich sand from the coast. Sands measured by Kasper-Zubillaga et al. (2007) near Golfo de Santa Clara were 83% quartz. Coastal sands probably influence the Gran Desierto far to the north of the eastern crescentic dunes where Kasper-Zubillaga et al. (2007) measured quartz abundance of 76%. In contrast, the spectral analysis here showed that nearby samples from the linear dunes farther north are more substantially influenced by local sources of feldspar, reducing the quartz concentration to an average of 61% (Fig. 1, *I).

The quartz mineralogy was best modeled by including in the end-member library both the monocrystalline quartz (BUR-4120) and cryptocrystalline quartz (or chert, analyzed at the IVIS laboratory). The quartz spectral library end member has a steeper feature at 9.1 μm (Fig. 2A), where this feature was slightly shallower in the sample spectra (Fig. 3A). The modeled spectra (Fig. 3A, shown as a dotted line) fit well to the measured spectra from these areas, but a residual error occurred at the main emissivity minima (9.1 µm or 1101 cm^{-1}), where the modeled emissivity values were roughly 1%–2% lower. The central dunes group was previously described as having a light-brown to reddish-yellow coloration resulting from iron-oxide coating (Blount and Lancaster, 1990). Scanning electron microscope (SEM) imaging determined that these grains have a small amount of iron- and magnesium-oxide coatings (Kennedy and Scheidt, 2010). However, spectral deconvolution of laboratory spectra did not detect hematite consistently. Chert has a slightly broader but similar spectral feature at 9.1 µm compared to the quartz spectral library end-member BUR-4120. Inclusion and exclusion of chert as an end member resulted in similar deconvolution results, where differences were expressed mainly as only a slightly higher RMS error between 0.001 and 0.004. Both quartz varieties had similar interpolated spatial patterns, where chert varied between 35% and 38% in the whole of the main dune field (Scheidt, 2009). Even though the data for the chert distribution

Downloaded from gsabulletin.gsapubs.org on June 7, 2011

showed a weak trend, chert may be a tracer for a unique sediment source. For example, similar to chert, quartzite and sandstone sources also have slightly different spectral features compared to monocrystalline quartz (Wenrich et al., 1995). Other possibilities for the small residual error at 9.1 µm of the spectra may be due to an older, desert-varnished source material of the dune sediments (Christensen and Harrison, 1993), particle-size effects (Hamilton, 1999), or unmodeled minerals. Based on these observations, the residual errors did not impact the spatial pattern of quartz-rich dune sediments.

Local Source Influences

In addition to the Colorado River sand source, local sources of sand have probably been an important and an abundant contemporaneous input of sand to the Gran Desierto. The Basin and Range mountains north of the Gran Desierto have widely varying lithology, ranging from older Proterozoic granites and gneiss to Tertiary basalts (Nourse et al., 2005). As source regions for eolian sediments, these areas contribute to the spectral variation of the dune sands, where the dominating effect is feldspar-rich sand derived from distal alluvial fans mixing with quartz-rich Colorado River sand. The minerals in the feldspar solution series have different spectral features, and several types of feldspar were included in the deconvolution of the laboratory spectra to explain grain variations. Likewise, single feldspar grains may exhibit intragrain variations in feldspar composition, meaning that a single mineral is less likely to represent a single source.

Albite was the most abundant feldspar found in samples located near the Sierra del Rosario and the Sierra Pinacate, followed by oligoclase. Albite and oligoclase had the same spatial patterns and had the greatest influence on the total feldspar spatial distribution (Scheidt, 2009). By comparing the composition from different geographic areas in the Gran Desierto to mineral abundances determined from geochemical studies of other regional dune fields, the degree of local source influence can be determined (Table 1). Feldspar increases with proximity to local sources, such as the alluvial fans of the Basin and Range Province, the Sierra del Rosario, and the Sonoyta dunes area. These areas reflect a bulk mineral composition profile similar to Mojave dune fields, such as the Kelso dunes (Ramsey et al., 1999), Bristol Trough, and Clark's Pass, where quartz abundance is low and total feldspar is high (Zimbelman and Williams, 2002).

Sierra del Rosario Dunes. Compared to the dunes heavily influenced by Colorado River sands, the dune sand south of the granitic Sierra del Rosario (Fig. 1, *C) had a lower average quartz (51%–67%) and higher total feldspar (33%–49%) concentration. Between the Sierra del Rosario and the central dunes area (Fig. 1, *D), eolian sediments admix with granitic material that originated from local alluvial sources. The spectra of local source–influenced sands had shallower emissivity spectra, and the quartz spectral feature at 9.1 µm was broader (Fig. 3C) because of the higher plagioclase feldspar content (38%), as well as potassium feldspar (as high as 9%) (Table 1, row C). Lithic concentration also was slightly higher near local sources, and the detection of volcanic grains was more common. The composition retrievals from dunes between the Sierra del Rosario and the alluvial fans of the Basin and Range (Fig. 1, *D) were clearly more influenced by local sources because quartz decreased to a range of 46%–60%, feldspar increased to 37%–57%, and total lithic abundance increased and was highly variable between 2% and 20% (Table 1, row D). According to the composition retrievals, most of the lithic content was modeled as ferrohornblende in this area.

Linear Dunes Northeast of the Sierra Pinacate. These dunes (Fig. 1, *I) are a group of vegetated linear dunes funneling between the southern extent of the Basin and Range alluvial fans and the northwestern margin of the Sierra Pinacate at the edge of the main sand sea. The compositional retrievals of the northern Pinacate (Table 1, row I) were very similar to the dunes that are south of the Sierra Pinacate (Fig. 1, *H; Table 1, row H). The most notable difference was the absence of potassium feldspar (Table 1) and an otherwise variable suite of feldspar end-member retrievals for these dunes. Dunes that are located in close proximity to

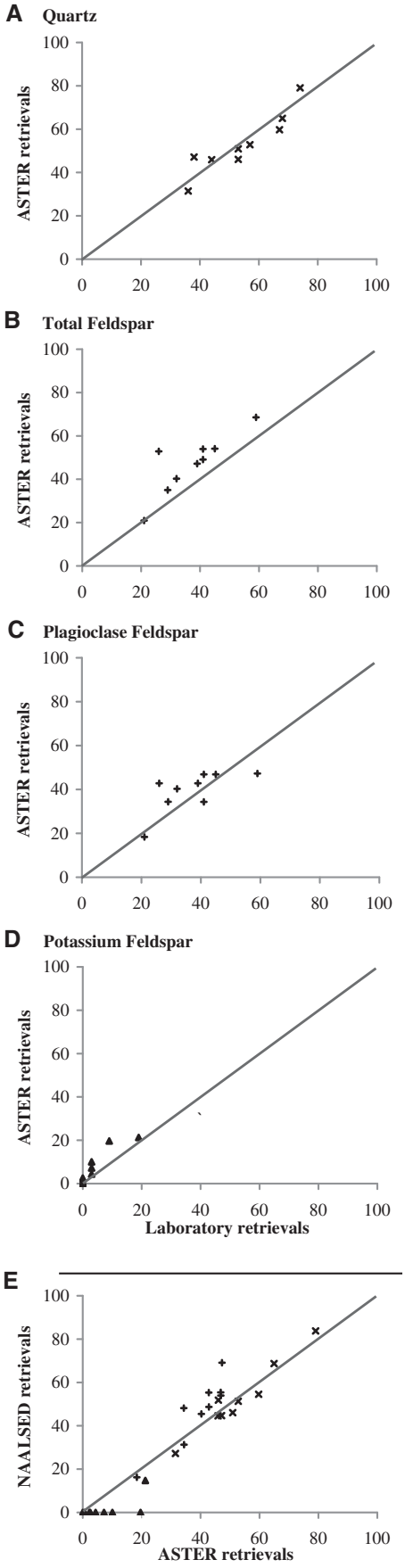

Figure 6. Average Advanced Spaceborne Thermal Emission and Reflection Radiometer (ASTER)–derived composition compared to composition derived from high-resolution laboratory spectra. Each ASTER retrieval is an average of the compositions determined from pixel locations where samples were collected. These values are compared directly to the averages of composition retrieved from individual samples according to the nine geographic locations reported in Table 1. Values are shown with respect to a 1:1 relationship (solid line). The ASTER mosaic data used in this study were also compared to retrievals from NAALSED mosaic data (E). "X" symbols refer to quartz, + indicates plagioclase, and filled triangles refer to potassium feldspar.

Downloaded from gsabulletin.gsapubs.org on June 7, 2011

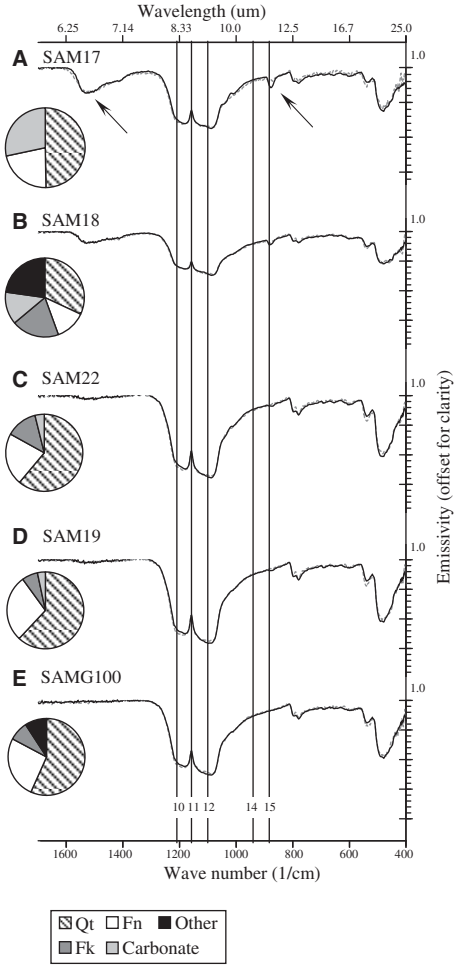

Figure 7. Sample spectra demonstrating the change in carbonate spectral features, i.e., loss of carbonate content, with transport distance from coastal sources. Arrows indicate characteristic spectral features of carbonate, where each pie chart to the left shows the relative proportions of total quartz (Qt), plagioclase feldspar (Fn), potassium feldspar (Fk), carbonate, and the total lithic content (Other). Decreasing carbonate abundance occurs with increasing transport distance from the coast in this order: (A) SAM17 and (B) SAM18 > (C) SAM22 > (D) SAM19 >> (E) SAMG100. A complete loss of carbonate occurs furthest from the carbonate source. Vertical lines show the position of Advanced Spaceborne Thermal Emission and Reflection Radiometer (ASTER) band-passes, where only band 14 is located in the area where a carbonate spectral feature is expressed.

alluvial fans of the Basin and Range and the Sierra Pinacate contain variable amounts of the anorthite spectral end member (a calcium feldspar), but content here reached as high as 20%. Previous field observations report labradorite (spectrally similar to anorthite) in Gran Desierto sands surrounding the Sierra Pinacate (Blount et al., 1990).

Sonoyta Dunes. The dunes that exist east and southeast of the Sierra Pinacate are a group of mostly linear and parabolic dunes that are mostly vegetated, but field observations clearly show signs of recent activity (Fig. 1, *G). These dune sands were characterized by high feldspar content (>55%). Coastal sands are the most likely source of quartz-rich sand, but the most likely feldspar-rich sediment source for the Sonoyta dunes is the ephemeral Sonoyta River, which passes through the coastal plain to the Gulf of California southeast of the Sierra Pinacate. Dunes exist on either side of the channel, and the morphology of the dunes suggests a coastal source of sand and/or reworking of the Sonoyta River sands. The spectral features of the average sample spectra were shallow, and the spectral feature at 9.1 µm was significantly broadened by potassium feldspar and was a different shape compared to other Gran Desierto spectra (Fig. 3G). Quartz content was lowest and total feldspar was highest in these dunes (55%–68%), where 50% of the total feldspar was potassium feldspar. Ferrohornblende was also found in minor amounts (3%–5%). An examination of the spatial pattern from the ASTER satellite data south of the Sierra Pinacate and the Sierra Blanca (Fig. 5F, row 5, columns F–G) suggests a very clear sand composition mixing relationship between sources of sand from the east (the main sand sea) and west (Sonoyta dunes sand). The composition is between 3% and 17% potassium feldspar at this location. Sonoyta dunes sand has the greatest resemblance to the bulk mineralogy of Mojave sands, exhibiting low mineralogical maturity (Ramsey et al., 1999; Zimbelman and Williams, 2002; Muhs et al., 2003).

Sonoyta sediment was probably derived from surrounding source rocks that have a prevalence of potassium feldspar. The possible local sources include currently exposed and/or eroded granitic and metamorphic rocks related to the Sierra Blanca and trachyte deposits in the Sierra Pinacate. Potassium feldspar exists in source rocks near the Rosario and the northern Pinacate dunes as well (e.g., Sierra del Choclo Doro), and yet laboratory analysis revealed less-abundant potassium feldspar. Sonoyta dune areas are able to maintain feldspar minerals because they are topographically isolated from the Colorado River sediment source ,which would otherwise dilute feldspar concentration with high quartz content, slowing the rate of mineralogical maturity. The Sonoyta dune area could represent an older, potassium-feldspar–rich local source of sands that have a low level of sediment reworking and are similar to Mojave dune fields in the Basin and Range Province.

Coastal Dunes. A significant amount of spectral variability was found in the samples collected along the coast of the Gran Desierto (Figs. 3E and 3F). Individual samples from this area range between 9% and 53% carbonate (Table 1, row E), but the spatially averaged value was decreased by other high-quartz-content samples from active patches of quartz-rich dunes in the area (Table 1, row F). A significant amount of variability in dune geomorphology exists in this area. In general, the area is an extensive vegetated sand sheet with coppice, linear, and a few star dunes punctuated by smaller units of active quartz-rich simple crescentic dunes that appear to migrate in a northerly direction. This area is further complicated by vegetated marshy coves and inlets, eroded fluvial deltaic deposits, sabkhas, and evaporite-rich playas. One laboratory spectrum of a sand sample indicated a very high abundance of gypsum (44%). This sand originated from nearby gypsiferous playas; this was detected and was easily spectrally distinguishable by ASTER. Similar in hardness to carbonate, these grains do not survive transport farther inland to the main dune field. In coastal areas, other lithics were detectable but were low in abundance, unlike samples near alluvial fans in the north. Some samples of coastal sands from beach ridges were very quartz-rich (as high as 73%) and were spectrally identified in ASTER TIR imagery. These results suggest a general bimodal coastal sediment source that includes first, a less-mature biogenic carbonate-rich sediment source (Ives, 1959), probably from shallow-water sediments of the Bahia Adair, and a second source of quartz-rich sand that represents either remnants of reworked, older sand dunes or sand originating from quartz-rich neritic sands from the beach ridges along the Gulf of California.

Lithic Distribution. The bulk mineralogy was dominated by quartz and feldspars. Lithics are defined in this paper as non-quartzofeldspathic sand grains. These minerals were identified in low abundance, and examination of their spatial distributions was only possible with the laboratory results. Because local sources vary and accessory assemblages become more complex, minor constituents compete in the deconvolution algorithm for a small percentage of the total lithic fractional abundance. False detection of a minor constituent can occur due to random noise or errors in the acquired spectrum, and the practical limit of compositional retrievals is not less

Downloaded from gsabulletin.gsapubs.org on June 7, 2011

than 10%. With these considerations, the lithic compositional maps presented here are used with caution, but they show some unique, meaningful spatial trends. Total hornblende, an end member associated with local granitic sources, averaged 11% and was as high as 20% in the Sierra del Rosario dune area (Fig. 1, *D), but lithic abundance averages less than 5% throughout the rest of the dune field. The average amount of volcanic lithics was expected to be much higher for samples around the Sierra Pinacate, but the average south and east of the Sierra Pinacate was only 1%. An average of 3% was found in the Sierra del Rosario area. The map of average total lithic concentration includes carbonates. The influence of carbonate on the total lithic content can be clearly observed by comparing total lithic distribution (Fig. 4E) to the carbonate trends (Fig. 4F). The highest percentage of total lithics was clearly a function of biogenic carbonate (shells) in the Bahia del Adair, and, secondly, proximity to granitic sources.

CONCLUSIONS

This study provides improved, more accurate spatial patterns of silicate composition compared to previous studies of dune patterns and dune morphology data in the Gran Desierto. It reveals that correlations between dune type and composition exist in some cases, but distinct compositions characteristic of dune groups and eolian construction events appear less common, suggesting that in this area, many of the dune generations identified by their different morphologic characteristics were formed by reworking of preexisting sediments, rather than representing input of new sediment by migration of dunes into the area. In the Gran Desierto, eolian sand distribution is best represented by a continuum of intermixing of sands with different compositions and levels of mineralogical maturity. High maturity, according to Muhs (2004), applies to sand that either originates from quartz-rich material or weathering processes that enrich it in the more competent mineral components, such as quartz. The determination that sand has high mineralogical maturity implies the dune sand is older and has experienced a greater number of these cycles. However, it can be concluded here that understanding sand provenance and transport from dune composition in the Gran Desierto is a complex problem because a mature, quartz-rich sand source from the ancestral Colorado River mixes with locally derived feldspar-rich sand from the Basin and Range Province. According to the Muhs (2004) definition, mineralogical maturity is reduced near local sources that contribute feldspar to the dunes, especially along the alluvial fans of the Basin and Range Province surrounding the Rosario and Sierra Pinacate and in the Sonoyta dune areas. The compositions in these areas are similar to other inland dune fields within the Basin and Range Province. However, the definition poses some problems for the Gran Desierto. In the areas where quartz input is low and local feldspar input is high and the most abundant competent mineral, the upper end member of maturity could be considered feldspar-rich sand. The addition of a quartz-rich sediment source to a feldspar-rich dune field artificially creates the appearance of a maturing sand system, and vice versa. A determination of the effective mineralogical maturity of the entire system would suggest that the Gran Desierto as a whole is a product of the interaction between the two major different sand systems: the ancestral Colorado River sand and the local Basin and Range sands. The evidence suggests that a quartz-rich Colorado River sediment system continually competes with local source input from the north and east.

This study represents the combination of composition retrievals from (1) high-resolution TIR emission laboratory spectroscopy from the largest geographical set of sand samples from a sand sea and (2) spatially contiguous, mosaicked TIR remote-sensing data. The spatial scales of remote-sensing data and spatially interpolated point data at the field sampling scale were effectively integrated to accurately explain the bulk mineralogical trends, distinguishing quartz and feldspar compositions, which is a significant advantage over previous studies of the Gran Desierto. Because sand samples were collected from less than 5 mm depth, the results are limited to understanding only the present-day surface sediment dynamics because they do not describe stratigraphic relationships between dunes or the superposition of eolian bed forms. Each sample represents a small point measurement assumed to be representative of a broad area, which is a valid assumption in most parts of the dune field. Sand transport pathways were inferred for a much larger sand sea than had been previously accomplished using these techniques (Ramsey et al., 1999) because mosaicked satellite-based ASTER TIR data were used. Sand transport pathways of feldspar-rich sands in the Sonoran Desert were related to the Gran Desierto dune field for the first time by expanding the remote-sensing analysis to the Sonoyta dunes. This paper has demonstrated a comprehensive, quantitative approach to mapping dune composition, and the results contribute to a better understanding of eolian system composition, patterns of eolian construction events, and the trends of mineralogical maturity. The limitations of mapping composition using ASTER TIR data with these methods were set by the instrument's spectral resolution and the unity constraint imposed in the linear spectral unmixing approach. These techniques could be ideal for a dune field composed of 3–4 spectral end members (e.g., compositions), and the mapping techniques can be applied to other large dune fields such as the Sahara Desert and other planetary surfaces (Scheidt et al., 2010b) where field work is difficult or impossible.

ACKNOWLEDGMENTS

Funding for this research was provided through the National Aeronautics and Space Administration (NASA) Solid Earth and Natural Hazards program (grant NAG5-13730), the NASA Earth and Space Science Fellowship (NESSF) Program (grant NNX06-AF92H), and the ASTER Science Team. The authors thank Glynn Hulley, Dan Muhs, and Alan Gillespie for thoughtful reviews that greatly improved the manuscript.

REFERENCES CITED

Bandfield, J.L., Hamilton, V.E., and Christensen, P.R., 2000, A global view of Martian surface compositions from MGS-TES: Science, v. 287, no. 5458, p. 1626–1630, doi: 10.1126/science.287.5458.1626.

Bandfield, J.L., Edgett, K.S., and Christensen, P.R., 2002, Spectroscopic study of the Moses Lake dune field, Washington: Determination of compositional distributions and source lithologies: Journal of Geophysical Research, v. 107, no. E11, p. 5092, doi: 10.1029/2000JE001469.

Bandfield, J.L., Hamilton, V.E., Christensen, P.R., and McSween, H.Y., 2004, Identification of quartzofeldspathic materials on Mars: Journal of Geophysical Research, v. 109, p. E10009, doi: 10.1029/2004JE002290.

Beveridge, C.A., Kocurek, G., Ewing, R., Lancaster, N., Morthekai, P., Singhvi, A.K., and Mahan, S.A., 2006, Development of spatially diverse and complex dunefield patterns: Gran Desierto dune field, Sonora, Mexico: Sedimentology, v. 53, no. 6, p. 1391–1409, doi: 10.1111/j.1365-3091.2006.00814.x.

Blount, G., and Lancaster, N., 1990, Development of the Gran Desierto sand sea, northwestern Mexico: Geology, v. 18, p. 724–728, doi: 10.1130/0091-7613(1990)018<0724:DOTGDS>2.3.CO;2.

Blount, G., Smith, M.O., Adams, J.B., Greeley, R., and Christensen, P.R., 1990, Regional aeolian dynamics and sand mixing in the Gran Desierto: Evidence from Landsat Thematic Mapper images: Journal of Geophysical Research, v. 95, p. 15,463–15,482, doi: 10.1029/JB095iB10p15463.

Byrnes, J.M., Ramsey, M.S., King, P.L., and Lee, R.J., 2007, Thermal infrared reflectance and emission spectroscopy of quartzofeldspathic glasses: Geophysical Research Letters, v. 34, L01306, doi: 10.1029/2006GL027893.

Christensen, P.R., and Harrison, S.T., 1993, Thermal infrared emission spectroscopy of natural surfaces: Application to desert varnish coatings on rocks: Journal of Geophysical Research, v. 98, no. B11, p. 19,819–19,834, doi: 10.1029/93JB00135.

Christensen, P.R., Bandfield, J.L., Smith, M.D., Hamilton, V.E., and Clark, R.N., 2000, Identification of a basaltic component on the Martian surface from thermal emission spectrometer data: Journal of Geophysical Research, v. 105, p. 9609–9621, doi: 10.1029/1999JE001127.

Christensen, P.R., Bandfield, J.L., Hamilton, V.E., Ruff, S.W., Mehall, G.L., Gorelick, N., Bender, K., Murray, K., Kieffer, H.H., and Titus, N.T., 2001, *Global Surveyor* thermal emission spectrometer experiment: Investigation description and surface science results:

Downloaded from gsabulletin.gsapubs.org on June 7, 2011

Journal of Geophysical Research, v. 106, no. E10, p. 23,823–23,871, doi: 10.1029/2000JE001370.

Christensen, P.R., Jakosky, B.M., Kieffer, H.H., Malin, M.C., McSween, H.Y., Jr., Nealson, K., Mehall, G.L., Silverman, S.H., Ferry, S., Caplinger, M., and Ravine, M., 2004, The Thermal Emission Imaging System (THEMIS) for the Mars 2001 *Odyssey* mission: Space Science Reviews, v. 110, p. 85–130, doi: 10.1023/B:SPAC.0000021008.16305.94.

Clarke, M.L., and Rendell, H.M., 1998, Climate change impacts on sand supply and the formation of desert sand dunes in the south-west USA: Journal of Arid Environments, v. 39, p. 517–531, doi: 10.1006/jare.1997.0372.

Colleta, B., and Ortlieb, L., 1984, Deformations of middle and late Pleistocene deltaic deposits at the mouth of the Rio Colorado, northwestern Gulf of California, *in* Malpica-Cruz, V., Celis-Gutiérrez, S., Guerrero-Garcia, J., and Ortlieb, L., eds., Neotectonics and Sea Level Variations in the Gulf of California Area: A Symposium: México, D.F., Instituto de Geologia, University Nacional Autónoma de México, p. 31–53.

Crowley, J.K., and Hook, S.J., 1996, Mapping playa evaporite minerals and associated sediments in Death Valley, California, with multispectral thermal infrared images: Journal of Geophysical Research, v. 101, no. B1, p. 643–660, doi: 10.1029/95JB02813.

Davis, J.C., 1986, Statistics and Data Analysis in Geology (2nd ed.): New York, John Wiley and Sons, 646 p.

Derickson, D., Kocurek, G., Ewing, R.C., and Bristow, C., 2008, Origin of a complex and spatially diverse dune-field pattern, Algodones, southeastern California: Geomorphology, v. 99, p. 186–204, doi: 10.1016/j.geomorph.2007.10.016.

Edgett, K.S., Ramsey, M.S., and Christensen, P.R., 1995, Aeolian erosion, transport, and deposition of volcaniclastic sands among the Shifting Sand Dunes, Christmas Lake, Oregon: TIMS image analysis, *in* Realmuto, V.J., ed., Summaries, Fifth Annual Airborne Earth Science Workshop, Volume 2: Pasadena, California, Jet Propulsion Laboratory Publication 95–1, p. 13–16.

Ewing, R.C., McElroy, B.J., and Andrews, B.J., 2007, Point pattern analysis of Star-Dune Fields: [abs.]: Eos (Transactions, American Geophysical Union), v. 88, no. 52, abstract NG41C–0673.

Feely, K.C., and Christensen, P.R., 1999, Quantitative compositional analysis using thermal emission spectroscopy: Application to igneous and metamorphic rocks: Journal of Geophysical Research, v. 104, no. E10, p. 24,195–24,210, doi: 10.1029/1999JE001034.

Gillespie, A.R., 1992a, Spectral mixture analysis of multispectral thermal infrared images: Remote Sensing of Environment, v. 42, p. 137–145, doi: 10.1016/0034-4257(92)90097-4.

Gillespie, A.R., 1992b, Enhancement of multispectral thermal infrared images: Decorrelation contrast stretching: Remote Sensing of Environment, v. 42, p. 147–155, doi: 10.1016/0034-4257(92)90098-5.

Gillespie, A.R., and Kahle, A.B., 1977, Construction and interpretation of a digital thermal inertia image: Photogrammetric Engineering and Remote Sensing, v. 43, no. 8, p. 983–1000.

Gillespie, A., Rokugawa, S., Matsunaga, T., Cothern, J.S., Hook, S.J., and Kahle, A.B., 1998, A temperature and emissivity separation algorithm for Advanced Spaceborne Thermal Emission and Reflection Radiometer (ASTER) images: IEEE Transactions on Geoscience and Remote Sensing, v. 36, p. 1113–1126, doi: 10.1109/36.700995.

Greeley, R., and Iversen, J.D., 1985, Wind as a Geologic Process: On Earth, Mars, Venus and Titan: Cambridge, UK, Cambridge University Press, p. 1–32.

Gustafson, W.T., Gillespie, A.R., and Yamada, G.J., 2006, Revisions to the ASTER temperature/emissivity separation algorithm, *in* Sobrino, J.A., ed., Recent Advances in Quantitative Remote Sensing: Torrent, Spain, Global Change Unit, University of Valencia.

Gutmann, J.T., and Sheridan, M.F., 1978, Geology of the Pinacate Volcanic Field: Arizona Bureau of Geology and Mineral Technology Special Paper 2, p. 47–59.

Hamilton, V.E., 1999, Particle size effects in particulate rock samples—Implications for thermal emission spectrometer (TES) data analysis in high albedo regions of Mars, *in* Fifth International Conference on Mars, 19–24 July 1999: Pasadena, California, abstract 6159.

Hamilton, V.E., and Christensen, P.R., 2000, Determining the modal mineralogy of mafic and ultramafic igneous rocks using thermal emission spectroscopy: Journal of Geophysical Research, v. 105, no. E4, p. 9717–9733, doi: 10.1029/1999JE001113.

Hamilton, V.E., Christensen, P.R., and McSween, H.Y., 1997, Determination of Martian meteorite lithologies and mineralogies using vibrational spectroscopy: Journal of Geophysical Research, v. 102, v. E11, p. 25,593–25,603.

Hamilton, V.E., Wyatt, M.B., McSween, H.Y., Jr., and Christensen, P.R., 2001, Analysis of terrestrial and Martian volcanic compositions using thermal emission spectroscopy: 2. Application to Martian surface spectra from the *Mars Global Surveyor* thermal emission spectrometer: Journal of Geophysical Research, v. 106, no. E7, p. 14,733–14,746, doi: 10.1029/2000JE001353.

Hamilton, V.E., Osterloo, M.M., and McGrane, B.S., 2007, THEMIS decorrelation stretched infrared mosaics for compositional evaluation of candidate 2009 Mars Science Laboratory landing sites: Houston, Texas, Lunar and Planetary Institute, Lunar and Planetary Science Conference XXXVIII, CD-ROM, abstract no. 1725.

Hapke, B., 1981, Bidirectional reflectance spectroscopy. 1: Theory: Journal of Geophysical Research, v. 86, p. 3039–3054.

Hewson, R.D., Cudahy, T.J., Mizuhiko, S., Ueda, K., and Mauger, A.J., 2005, Seamless geological map generation using ASTER in the Broken Hill–Curnamona province of Australia: Remote Sensing of Environment, v. 99, p. 159–172, doi: 10.1016/j.rse.2005.04.025.

Hook, S.J., Karlstrom, K.E., Miller, C.F., and McCaffrey, K.J.W., 1994, Mapping the Piute Mountains, California, with thermal infrared multispectral scanner (TIMS) images: Journal of Geophysical Research, v. 99, no. B8, p. 15,605–15,622, doi: 10.1029/94JB00690.

Hook, S.J., Myers, J.J., Thome, K.J., Fitzgerald, M., and Kahle, A.B., 2001, The MODIS/ASTER airborne simulator (MASTER)—A new instrument for earth science studies: Remote Sensing of Environment, v. 76, no. 1, p. 93–102, doi: 10.1016/S0034-4257(00)00195-4.

Hulley, G.C., and Hook, S.J., 2009, The North American ASTER Land Surface Emissivity Database (NAALSED) Version 2.0: Remote Sensing of Environment, v. 113, p. 1967–1975, doi: 10.1016/j.rse.2009.05.005.

Hulley, G.C., Hook, S.J., and Baldridge, A.M., 2008, ASTER Land Surface Emissivity Database of California and Nevada: Geophysical Research Letters, v. 35, p. L13401, doi: 10.1029/2008GL034507.

Hulley, G.C., Hook, S.J., and Baldridge, A.M., 2009, Validation of the North American ASTER Land Surface Emissivity Database (NAALSED), version 2.0, using pseudo-invariant sand dune sites: Remote Sensing of Environment, v. 113, no. 10, p. 2224–2233, doi: 10.1016/j.rse.2009.06.005.

Ives, R.L., 1959, Shell dunes of the Sonoran shore: American Journal of Science, v. 257, p. 449–457, doi: 10.2475/ajs.257.6.449.

Kahle, A.B., 1987, Surface emittance, temperature, and thermal inertia derived from thermal infrared multispectral scanner (TIMS) data for Death Valley, California: Geophysics, v. 52, p. 858–874, doi: 10.1190/1.1442357.

Kasper-Zubillaga, J.J., 2009, Roundness in quartz grains from inland and coastal dune sands, Altar Desert, Sonora, Mexico: Boletín de la Sociedad Geológica Mexicana, v. 61, no. 1, p. 1–12.

Kasper-Zubillaga, J.J., and Carranza-Edwards, A., 2005, Grain size discrimination between sands of desert and coastal dunes from northwestern Mexico: Revista Mexicana de Ciencias Geologicas, v. 22, no. 3, p. 383–390.

Kasper-Zubillaga, J.J., and Faustinos-Morales, R., 2007, Scanning electron microscopy analysis of quartz grains in desert and coastal dune sands: Ciencias Marinas, v. 33, no. 1, p. 11–22.

Kasper-Zubillaga, J.J., Zolezzi-Ruíz, H., Carranza-Edwards, A., Girón-García, P., Ortiz-Zamora, G., and Palma, M., 2007, Sedimentological, modal analysis and geochemical studies of desert and coastal dunes, Altar Desert, NW Mexico: Earth Surface Processes and Landforms, v. 32, p. 489–508, doi: 10.1002/esp.1402.

Kasper-Zubillaga, J.J., Acevedo-Vargas, B., Morton Bermea, O., and Ortiz-Zamora, G., 2008, Rare earth elements of the Altar Desert dune and coastal sands: Northwestern Mexico, Chemie der Erde-Geochemistry, v. 68, p. 45–59, doi: 10.1016/j.chemer.2006.05.001.

Katra, I., and Lancaster, N., 2008, Surface-sediment dynamics in a dust source from spaceborne multispectral thermal infrared data: Remote Sensing of Environment, v. 112, no. 7, p. 3212–3221, doi: 10.1016/j.rse.2008.03.016.

Katra, I., Scheidt, S.P., and Lancaster, N., 2009, Changes in active eolian sand at northern Coachella Valley, California: Geomorphology, v. 105, no. 3–4, p. 277–290, doi: 10.1016/j.geomorph.2008.10.004.

Kennedy, S.K., and Scheidt, S.P., 2010, Utilization of CCSEM methods to determine minor/accessory mineral abundances from inland desert dune sans of the Gran Desierto: Geological Society of America Annual Meeting Abstracts with Programs, v. 42, no. 5, p. 416.

Kirkland, L.E., Herr, K.C., and Salisbury, J.W., 2001, Thermal infrared spectral band detection limits for unidentified surface materials: Applied Optics, v. 40, p. 4852–4862, doi: 10.1364/AO.40.004852.

Kirkland, L.E., Herr, K.C., Keim, E., Adams, P., Salisbury, J.W., Hackwell, J., and Treiman, A., 2002, First use of an airborne thermal infrared hyperspectral scanner for compositional mapping: Remote Sensing of Environment, v. 80, p. 447–459, doi: 10.1016/S0034-4257(01)00323-6.

Kocurek, G., and Lancaster, N., 1999, Aeolian system sediment state: Theory and Mojave Desert Kelso dune field example: Sedimentology, v. 46, no. 3, p. 505–515, doi: 10.1046/j.1365-3091.1999.00227.x.

Kruse, F.L., and Raines, G.L., 1984, A technique for enhancing digital color images by contrast stretching in Munsell color space, *in* Proceedings of the International Symposium on Remote Sensing of Environment, Third Thematic Conference, Remote Sensing for Exploration Geology, Colorado Springs, Colorado, 16–19 April 1984: Ann Arbor, Michigan, Environmental Research Institute of Michigan, p. 309–324.

Lancaster, N., 1989, The dynamics of star dunes: An example from the Gran Desierto, Mexico: Sedimentology, v. 36, p. 273–289, doi: 10.1111/j.1365-3091.1989.tb00607.x.

Lancaster, N., 1992, Relations between dune generations in the Gran Desierto of Mexico: Sedimentology, v. 39, p. 631–644, doi: 10.1111/j.1365-3091.1992.tb02141.x.

Lancaster, N., 1993a, Origins and sedimentary features of supersurfaces in the northwestern Gran Desierto sand sea, *in* Pye, K., and Lancaster, N., eds., Eolian Sediments: Ancient and Modern: International Association of Sedimentology Special Publication 16, p. 71–83.

Lancaster, N., 1993b, Kelso dunes: National Geographic Research and Exploration, v. 9, p. 44–59.

Lancaster, N., 1994, Controls on aeolian activity: Some new perspectives from the Kelso dunes, Mojave Desert, California: Journal of Arid Environments, v. 27, p. 113–125.

Lancaster, N., 1995, Origin of the Gran Desierto sand sea, Sonora, Mexico: Evidence from dune morphology and sedimentology, *in* Tchakerian, V.P., ed., Desert Aeolian Processes: London, Chapman & Hall, p. 11–35.

Lancaster, N., Greeley, R., and Christensen, P.R., 1987, Dunes of the Gran Desierto sand sea, Sonora, Mexico: Earth Surface Processes and Landforms, v. 12, p. 277–288, doi: 10.1002/esp.3290120306.

Lynch, D.J., and Gutmann, J.T., 1990, Volcanic structure and alkaline rocks in the Pinacate volcanic field of Sonora, Mexico, *in* Gehrels, G.E., and Spencer, J.E., eds., Geologic Excursions through the Sonoran Desert Region, Arizona and Sonora: Arizona Geological Survey Special Paper 7, p. 309–322.

Martínez-Alonso, S., Jakosky, B.M., Mellon, M.T., and Putzig, N.E., 2005, A volcanic interpretation of Gusev crater surface materials from thermophysical, spectral and morphological evidence: Journal of Geophysical Research, v. 110, p. E01003, doi: 10.1029/2004JE002327.

May, L.A., 1973, Geological reconnaissance of the Gran Desierto region, northwestern Sonora, Mexico: Journal of the Arizona Academy of Science, v. 8, no. 3, p. 158–169, doi: 10.2307/40021779.

Downloaded from gsabulletin.gsapubs.org on June 7, 2011

McKee, E.D., 1979, Ancient sandstones considered to be eolian, *in* McKee, E.D., ed., A Study of Global Sand Seas: U.S. Geological Survey Professional Paper 1052, p. 187–233.

Merriam, R., and Bandy, O.L., 1969, Source of Upper Cenozoic sediments in the Colorado River delta region: Journal of Sedimentary Petrology, v. 35, p. 911–916.

Milam, K.A., McSween, H.Y., Hamilton, V.E., Moersch, J.M., and Christensen, P.R., 2004, Accuracy of plagioclase compositions from laboratory and Mars spacecraft thermal emission spectra: Journal of Geophysical Research, v. 109, p. E04001, doi: 10.1029/2003JE002097.

Muhs, D.R., 2004, Mineralogical maturity in dunefields of North America, Africa and Australia: Geomorphology, v. 59, no. 1–4, p. 247–269, doi: 10.1016/j.geomorph.2003.07.020.

Muhs, D.R., Bush, C.A., Cowherd, S.D., and Mahan, S., 1995, Geomorphic and geochemical evidence for the source of sand in the Algodones dunes, Colorado Desert, southeastern California, *in* Tchakerian, V.P., ed., Desert Aeolian Processes: London, Chapman & Hall, p. 37–74.

Muhs, D.R., Reynolds, R.L., Been, J., and Skipp, G., 2003, Eolian sand transport pathways in the southwestern United States: Importance of the Colorado River and local sources: Quaternary International, v. 104, p. 3–18, doi: 10.1016/S1040-6182(02)00131-3.

Mustard, J.F., and Pieters, C.M., 1988, Predicting mineral abundances from reflectance spectra: [abs.]: Houston, Texas, Lunar and Planetary Institute, Lunar Planetary Science Conference XIX, p. 825–826.

Nourse, J.A., Premo, W.R., Iriondo, A., and Stahl, E.R., 2005, Contrasting Proterozoic basement complexes near the truncated margin of Laurentia, northwestern Sonora-Arizona international border region, *in* Anderson, T.H., Nourse, J.A., McKee, J.W., and Steiner, M.B., eds., The Mojave-Sonora Megashear Hypothesis: Development, Assessment, and Alternatives: Geological Society of America Special Paper 393, p. 123–182, doi: 10.1130/0-8137-2393-0.123.

Ortega-Gutiérrez, F., Mitre-Salazar, L.M., Roldán-Quintana, J., Aranda-Gómez, J., Morán-Zenteno, D., and Nieto-Samaniego, A., 1992, Carta Geológica de la República Mexicana (Geologic Chart of the Mexican Republic): México, D.F., Instituto de Geología, Universidad Nacional Autónoma de México, scale 1:2,000,000.

Paisley, E.C.I., Lancaster, N., Gaddis, L.R., and Greeley, R., 1991, Discrimination of active and inactive sand from remote sensing: Kelso dunes, Mojave Desert, California: Remote Sensing of Environment, v. 37, p. 153–166, doi: 10.1016/0034-4257(91)90078-K.

Pease, P., and Tchakerian, V., 2003, Geochemistry of sediments from Quaternary sand ramps in the southeastern Mojave Desert, California: Quaternary International, v. 104, p. 19–29, doi: 10.1016/S1040-6182(02)00132-5.

Pease, P.P., Bierly, G.D., Tchakerain, V.P., and Tindale, N.W., 1999, Mineralogical characterization and transport pathways of dune sand using Landsat TM data, Wahiba Sand Sea, in the Central Taklimakan sand sea: Sedimentary Geology, v. 161, p. 1–14.

Ramsey, M.S., 2002, Ejecta distribution patterns at Meteor crater, Arizona: On the applicability of lithologic end-member deconvolution for spaceborne thermal infrared data of Earth and Mars: Journal of Geophysical Research, v. 107, no. E8, doi: 10.1029/2001JE001827.

Ramsey, M.S., and Christensen, P.R., 1998, Mineral abundance determination: Quantitative deconvolution of thermal emission spectra: Journal of Geophysical Research, v. 103, p. 577–596, doi: 10.1029/97JB02784.

Ramsey, M.S., and Rose, S., 2010, The complex effects of subpixel compositional, thermal and textural heterogeneities on spaceborne TIR data, *in* 2nd HyspIRI Science Workshop, 9–12 May 2010: Pasadena, California.

Ramsey, M.S., Christensen, P.R., Lancaster, N., and Howard, D.A., 1999, Identification of sand sources and transport pathways at the Kelso dunes, California, using thermal infrared remote sensing: Geological Society of America Bulletin, v. 111, p. 646–662, doi: 10.1130/0016-7606(1999)111<0646:IOSSAT>2.3.CO;2.

Realmuto, V., 1990, Separating the effects of temperature and emissivity: Emissivity spectrum normalization, *in* Abbott, E.A., ed., Proceedings of the Second Annual Airborne Earth Science Workshop, Volume 2: Jet Propulsion Laboratory Publication 90–55, p. 31–35.

Richards, J.A., 1999, Remote Sensing Digital Image Analysis: An Introduction: Berlin, Germany, Springer-Verlag, 240 p.

Rowan, L.C., and Mars, J.C., 2003, Lithologic mapping in the Mountain Pass, California, area using Advanced Spaceborne Thermal Emission and Reflection Radiometer (ASTER) data: Remote Sensing of Environment, v. 84, p. 350–366, doi: 10.1016/S0034-4257(02)00127-X.

Rowan, L.C., Mars, J.C., and Simpson, C.J., 2005, Lithologic mapping of the Mordor, NT, Australia, ultramafic complex by using the Advanced Spaceborne Thermal Emission and Reflection Radiometer (ASTER): Remote Sensing of Environment, v. 99, p. 105–126, doi: 10.1016/j.rse.2004.11.021.

Ruff, S.W., 1998, Quantitative Thermal Emission Spectroscopy Applied to Granitoid Petrology, [Ph.D. dissertation]: Tempe, Arizona, Arizona State University, 234 p.

Ruff, S.W., Christensen, P.R., Barbera, P.W., and Anderson, D.L., 1997, Quantitative thermal emission spectroscopy of minerals: A laboratory technique for measurement and calibration: Journal of Geophysical Research, v. 102, p. 14,899–14,913, doi: 10.1029/97JB00593.

Scheidt, S.P., 2009, Aeolian System Dynamics Derived from Thermal Infrared Data [Ph.D. dissertation]: Pittsburgh, Pennsylvania, University of Pittsburgh, 291 p.

Scheidt, S.P., Ramsey, M.S., and Lancaster, N., 2006, Fusion of multitemporal/multispectral satellite data for the Gran Desierto: Implications for long distance sand transport, *in* Nickling, W.G., Turner, S., Gillies, J.A., and Puddister, M, eds., Sixth International Conference on Aeolian Research Program and Abstracts, 24–26 July 2006: Ontario, Canada, University of Guelph, 86 p.

Scheidt, S.P., Ramsey, M.S., and Lancaster, N., 2008, Radiometric normalization and image mosaic generation of ASTER thermal infrared data: An application to extensive sand sheets and dune fields: Remote Sensing of Environment, v. 112, p. 920–933, doi: 10.1016/j.rse.2007.06.020.

Scheidt, S.P., Lancaster, N. and Ramsey, M.S., 2010a, Sand composition of the Gran Desierto: A terrestrial analogue for thermal infrared imaging and spectroscopy techniques, *in* Second International Planetary Dunes Workshop: abstract 2010.

Scheidt, S.P., Ramsey, M.S., Mohummad, R., Mercurio, E., and Lancaster, N., 2010b, Performance of the proposed HyspIRI TIR bands for accurate compositional identification of eolian dust, ash and sand, *in* 3rd HyspIRI Science Workshop, 24–26 August 2010: Pasadena, California.

Sharp, R.P., 1966, Kelso dunes, Mojave Desert, California: Geological Society of America Bulletin, v. 77, p. 1045–1077, doi: 10.1130/0016-7606(1966)77[1045:KDMDC]2.0.CO;2.

Shipman, H., and Adams, J.B., 1987, Detectability of minerals on desert alluvial fans using reflectance spectra: Journal of Geophysical Research, v. 92, p. 10,391–10,402, doi: 10.1029/JB092iB10p10391.

Smith, R.S.U., 1982, Sand dunes in the North American deserts, *in* Bender, G.L., ed., Reference Handbook on the Deserts of North America: Westport, Connecticut, Greenwood Press, p. 481–524.

Tchakerian, V.P., 1991, Late Quaternary aeolian geomorphology of the Dale Lake sand sheet, southern Mojave Desert, California: Physical Geography, v. 12, p. 347–369.

Tchakerian, V.P., and Lancaster, N., 2002, Late Quaternary arid/humid cycles in the Mojave Desert and western Great Basin of North America: Quaternary Science Reviews, v. 21, p. 799–810, doi: 10.1016/S0277-3791(01)00128-7.

Thome, K., Palluconi, F., Takashima, T., and Masuda, K., 1998, Atmospheric correction of ASTER: IEEE Transactions on Geoscience and Remote Sensing, v. 36, no. 4, p. 1199–1211, doi: 10.1109/36.701026.

Thomson, J.L., and Salisbury, J.W., 1993, The mid-infrared reflectance of mineral mixtures (7–14 μm): Remote Sensing of Environment, v. 45, p. 1–13, doi: 10.1016/0034-4257(93)90077-B.

Watkins, T., 2003, Geologic History of Proterozoic Basement in the Area of Desierto de Altar, Sonora, Mexico, near Sierra Los Ojos; with Possible Relations to the Rodinia Supercontinent [Senior thesis]: Pomona, California, California State Polytechnic University, 42 p.

Wenrich, M.L., Hamilton, V.E., and Christensen, P.R., 1995, A field- and laboratory-based quantitative analysis of alluvium: Relating analytical results to TIMS data, *in* Realmuto, V.J., ed., Summaries of the Fifth Annual JPL Airborne Earth Science Workshop, Volume 2, TIMS Workshop: Pasadena, California, Jet Propulsion Laboratory, p. 39–42 (see N95–33789 12–42).

Winspear, N.R., and Pye, K., 1995, Sand supply to the Algodones dunefield, south-eastern California, USA: Sedimentology, v. 42, p. 875–891, doi: 10.1111/j.1365-3091.1995.tb00415.x.

Wood, C.A., 1974, Reconnaissance geophysics and geology of the Pinacate craters, Sonora, Mexico: Bulletin of Volcanology, v. 38, p. 149–172, doi: 10.1007/BF02597808.

Wright, S.P., and Ramsey, M.S., 2006, Thermal infrared data analyses of Meteor crater, Arizona: Implications for Mars spaceborne data from the Thermal Emission Imaging System: Journal of Geophysical Research, v. 111, no. E8, doi: 10.1029/2005JE002472.

Wyatt, M.B., and McSween, H.Y., Jr., 2002, Spectral evidence for weathered basalt as an alternative to andesite in the northern lowlands of Mars: Nature, v. 417, p. 263–266, doi: 10.1038/417263a.

Yamaguchi, Y., Kahle, A., Tsu, H., Kawakami, T., and Pniel, M., 1998, Overview of the Advanced Spaceborne Thermal Emission and Reflectance Radiometer (ASTER): IEEE Transactions on Geoscience and Remote Sensing, v. 36, p. 1062–1071, doi: 10.1109/36.700991.

Zimbelman, J.R., and Williams, S.H., 2002, Geochemical indicators of separate sources for eolian sands in the eastern Mojave Desert, California, and western Arizona: Geological Society of America Bulletin, v. 114, no. 4, p. 490–496, doi: 10.1130/0016-7606(2002)114<0490:GIOSSF>2.0.CO;2.

Zimbelman, J.R., Williams, S.H., and Tchakerian, V.P., 1995, Sand transport paths in the Mojave Desert, southwestern United States, *in* Tchakerian, V.P., ed., Desert Aeolian Processes: New York, Chapman and Hall, p. 101–129.

Manuscript Received 26 May 2010
Revised Manuscript Received 8 September 2010
Manuscript Accepted 24 September 2010

Printed in the USA